The DUNE-PRISM Near Detector

T. Cai[1], J. Calcutt[2], K. Mahn[2], L. Pickering[2], S. Manly[1], H. Tanaka[3], C. Vilela[4], M. Wilking[4], and G. Yang[4]

[1]University of Rochester
[2]Michigan State University
[3]SLAC National Accelerator Laboratory
[4]Stony Brook University

January 25, 2018

Contents

1 Introduction

As long-baseline neutrino experiments move into the high precision era, one of the most difficult challenges will be to control systematic uncertainties due to neutrino interaction modeling. The relationship between the observable final state particles from a neutrino interaction on liquid argon (LAr) and the incident neutrino energy is currently not understood with sufficient precision to achieve DUNE physics goals due to missing energy from undetected particles (such a neutrons and low energy charged pions) and misidentified particles. This causes a “feed-down” in reconstructed neutrino energy relative to the true energy. Since neutrino energy spectra at the far and near detectors are very different, given what is currently known about neutrino oscillation parameters, due to the presence of oscillations at the far detector, these neutrino energy feed-down effects do not cancel in a far/near ratio as a function of neutrino energy, and lead to biases in the measured oscillation parameters.

Neutrino energy estimation depends on the interaction model in two ways [1]. First, any undetected charged pions will cause the energy estimation to be incorrect by at least the pion mass, so the energy estimator is reliant on the predicted multiplicity and kinematics of mesons as they couple to detection threshold. Second, the neutrons produced in neutrino interactions will induce multiple interactions per neutron, and the detector response of a these neutron interactions is not well correlated to the kinetic energy carried by the primary neutron emerging from the argon nucleus, so it is not evident DUNE will be able to detect the multiplicity or energy of neutrons. Energy lost to neutrons can be quite different between neutrino and antineutrino interactions, and will contribute to a biased energy estimator. Studies done by other groups, consistent with the studies done in this note, indicate that missing energy and/or incorrect modelling can result in bias in oscillation parameters, especially δ_{CP} [2, 3]; we perform similar studies here with similar conclusions. In the T2K experiment, neutrino interaction model uncertainties are currently the dominant systematic uncertainty (nearly 3.9% of the 5.0% total error budget for the ν_e rate) [4].

Constraining neutrino interaction uncertainties is particularly difficult, since no complete model of neutrino interactions is available. If it were possible to construct a model that was known to be correct, even with a large number of unknown parameters, then the task of a near detector would much simpler: to build a detector that can constrain the unknown parameters of the model. However, in the absence of such a model, such a strategy will be subject to unknown biases due to the interaction model itself, which are difficult to constrain.

One strategy to understand the potential impact of using imperfect neutrino interaction models is to produce fake datasets that include modifications to the neutrino interaction cross sections that are unknown to the model being used to fit the fake data. In this way, it is possible to understand potential biases in oscillation parameters extracted from a full near+far detector fit due to the use of an incorrect cross section model in the fit. One such fake data study will be presented in this note.

The DUNE-PRISM near detector concept can provide a data-driven determination of the relationship between true and reconstructed energy that is significantly less sensitive to neutrino interaction models. This technique consists of a movable LAr detector that can measure the neutrino beam at a variety of off-axis angles. Since the peak neutrino energy decreases as the observation angle relative to the beam direction increases, as shown in Figure Figure 1b, off-axis measurements provide an additional degree of freedom for separating systematic effects from the neutrino flux prediction and neutrino interaction modeling. The flux at each off-axis position can roughly be thought of as a set of states with different peak energies over the energy range that is sampled, which can be transformed via linear combinations to a set of nearly Gaussian energy spectra. This allows for a direct mapping of true energy (from the Gaussian flux) to reconstructed energy (from the chosen observables in the detector). This relationship can then be inverted at the far detector to extract the true neutrino energy spectrum from the same observables. In addition to Gaussian fluxes, predicted energy spectra at the far detector can be produced directly from linear combinations of off-axis measurements at the near detector for any set of oscillation parameters. This provides a far detector prediction that is largely independent of neutrino interaction modeling.

This note will present the current status of the off-axis flux fits to produce Gaussian and oscillated spectra, an initial set of studies on the impact of flux systematic errors, an example run plan with event rates for off-axis measurements with detector selection efficiencies applied, and a fake data study showing an example of a biased measurement of oscillation parameters if only on-axis near detector measurements are performed. The next steps consist of a full oscillation analysis with far detector predictions produced directly from linear combinations of DUNE-PRISM off-axis measurements.

2 Linear Combinations of Off-axis Neutrino Fluxes

The DUNE-PRISM suite of measurements allows for the use of linear combinations of multiple measurements, taken under exposure to different neutrino fluxes, to closely approximate a single measurement taken in some other neutrino flux of interest. In this way, the near detector of an oscillation experiment can be effectively exposed to the approximately same neutrino flux as the far detector—allowing for a more direct comparison of near and far event rate differences. This can result in a very significant de-coupling of the flux and neutrino interaction uncertainties that otherwise are difficult to disentangle when using measurements from a near detector—exposed to an unoscillated neutrino flux—to predict the distribution of any reconstructed observable (e.g. reconstructed neutrino energy) at a far detector. The original implementation was proposed by the NuPRISM collaboration for use as a next-generation near-detector for the long baseline oscillation experiments based at J-PARC, Japan [5].

The practical implementation of the technique makes use of the "off-axis effect", which is a result of the angular dependence of the decay kinematics of relativistic particles. Specifically, the relationship between the energy of the decay parent particle and the final state neutrino energy changes as a function of observation angle away from the parent boost direction; this can be seen in Figure 1a. The NOνA and T2K long-baseline oscillation experiments already use this feature—often called 'the off axis effect'—to achieve a more narrowly peaked neutrino energy spectrum than can be achieved by a purely on-axis experiment.

The neutrino flux prediction for a number of off-axis positions for a near detector at 575 m from the target station are shown in Figure 1b[1]. For reference, at 575 m, a 1 m lateral shift corresponds to approximately a 0.1° change in off-axis angle.

To form a desired neutrino energy spectra, the off-axis measurements are linearly combined. The coefficients for each off-axis measurement in the linear sum are determined by fitting the linearly combined spectra to some target spectra—*e.g.* the oscillated far detector flux (§ 2.3) or quasi-monoenergetic fluxes (§ 2.2). Quasi-monoenergtic measurements can be can be used to 'calibrate' the relationship between neutrino energy and observed energy.

[1]The simulation specifics are described in Appendix A.

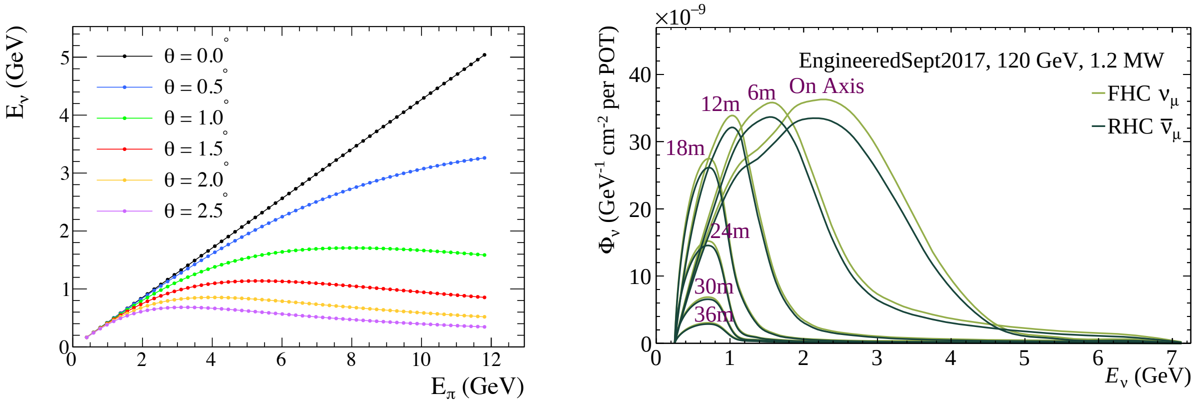

(a) Off-axis pion decay kinematics

(b) DUNE near detector flux predictions

Figure 1: (a) The neutrino energy as a function of parent pion energy for different angles away from the pion momentum vector. Figure from Ref. [11]. (b) The DUNE near detector flux predictions over a range of off-axis positions for a near detector at 575 m downstream of the target station.

2.1 DUNE neutrino flux

The neutrino beam used for DUNE will be provided by the LBNF at FNAL. The beamline simulation used to generate the flux predictions used in this document, `g4lbnf`, is described in detail elsewhere [6]. The predictions presented in this section, § 4, and § 5 were all simulated with `g4lbnf v3r5p3`.

2.1.1 Flux predictions

`g4lbne`[2] simulates the propagation and subsequent hadronization of beam protons as they impact the DUNE target. Interaction products are then propagated through the target and horn geometries and into the decay pipe until they decay to produce neutrinos. For a given decaying neutrino parent particle, the probability that the boosted, final state neutrino will be produced with a momentum vector pointing towards an arbitrary point in space can be calculated. In this way, the simulated neutrino can be forced to pass through some relevant flux window and then weighted with this calculated probability. This greatly increases the computational efficiency for producing high statistics neutrino flux predictions at a range of relevant off-axis near detector positions. The predicted off-axis neutrino flux spectra for muon neutrinos in a neutrino-mode beam are shown in Figure 1b. These predictions assume that the near detector is taking measurements in 10 cm(W) $\times$ 4 m(L) $\times$ 2 m(H) slices at a distance of 575 m from the target. The down-shift in peak neutrino energy with increasing off-axis position—as expected from Figure 1a—can be clearly seen. This is accompanied by overall reduction in integrated flux because of the available rest-frame phase space for producing boosted neutrinos observable at large off-axis positions.

It is also interesting to examine how the predicted, intrinsic neutrino flavor-content of the beam varies with off-axis angle. Figure 2a shows the neutrino-mode, or Forward Horn

[2] The package is now called `g4lbnf`, but the executable is still, historically named `g4lbne`.

Alignment parameter	Tolerance
Horn current	3kA
Horn 1 position	0.5mm
Horn 2 position	0.5mm
Target position	0.5mm
Decay pipe radius	0.1m
Horn water layer thickness	0.5mm
Baffle scraping	0.25%

Table 1: The tolerances used in the beam systematic uncertainty study presented in Ref. [10].

Current (FHC), and anti-neutrino-mode (RHC) predictions for the four neutrino flavors at the on-axis position, and a moderately off-axis position. At the 30 m position, a second, smaller energy peak that is evident. By separating the flux prediction by decay parent species, it is clear that this peak arises from charged kaon neutrino parents—where the main flux peak comes from charged pion parents. As with the pion-parent peak, the kaon-parent peak is significantly narrower in observed neutrino energy at greater off-axis angle, which may allow for off-axis kaon-parent analyses.

The full FHC muon neutrino flux prediction, as a function of off-axis position and neutrino energy is shown in Figure 3.

2.1.2 Beam focussing uncertainties

The effect of the most relevant sources of beam focussing error, as determined in Ref. [10], were extended to the off-axis flux predictions. The tolerances used here were informed by Table 1, with the exception of the the '1 σ' uncertainty on the horn current, which was taken as 2 kA, as in Ref. [12]. See § 3 for a complementary study on the off-axis dependence of errors in the horn alignment.

Figure 4 shows the response of the on-axis flux predictions to variations of the decay pipe radius, water layer thickness, and horn current. These agree well with the corresponding uncertainties calculated by beam-group studies, *e.g.* Figure 5.

The response to focussing error variations as a function of both off-axis position and neutrino energy can be seen in Figure 6. The significant variation shown in the top right pane correspond to a 3 σ shift in horn current—as defined by the official beam-group tolerances [10].

2.1.3 Hadronization uncertainties

The production of pions and kaons, and their re-interactions, are significant sources of uncertainty in the flux prediction [10]. Unfortunately, at the time of writing, the software for

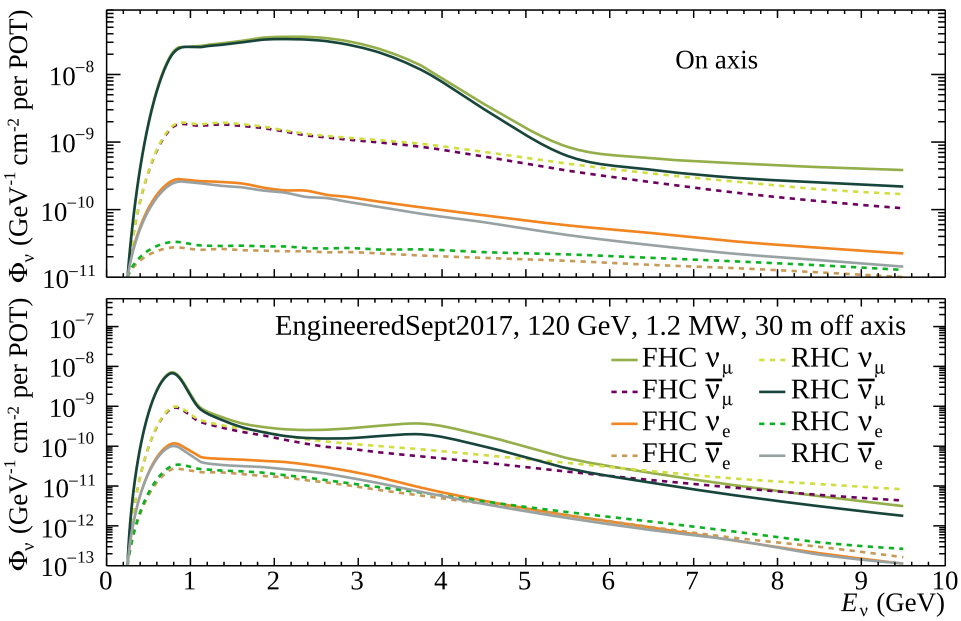

(a) Beam neutrino flavor content

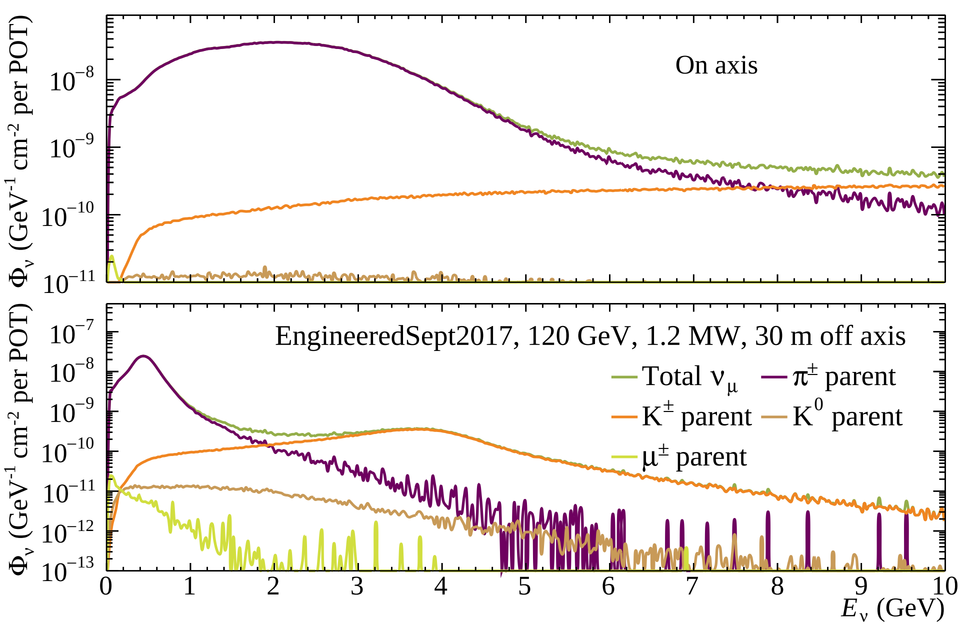

(b) Beam neutrino decay-parent species

Figure 2: The predicted muon neutrino energy spectra at two near detector positions, on axis and 30 m off axis. (a) The predicted neutrino flavor-content of the neutrino-mode (FHC) and anti-neutrino-mode (RHC) beam. (b) The neutrino-mode, muon-flavor predicted flux, separated by the particle that decayed to produce the neutrino. The off-axis spectrum displays a double peak structure due to charged kaon parent decay kinematics. The on-axis kaon-peak occurs at higher neutrino energy and will have a significantly broader energy spread.

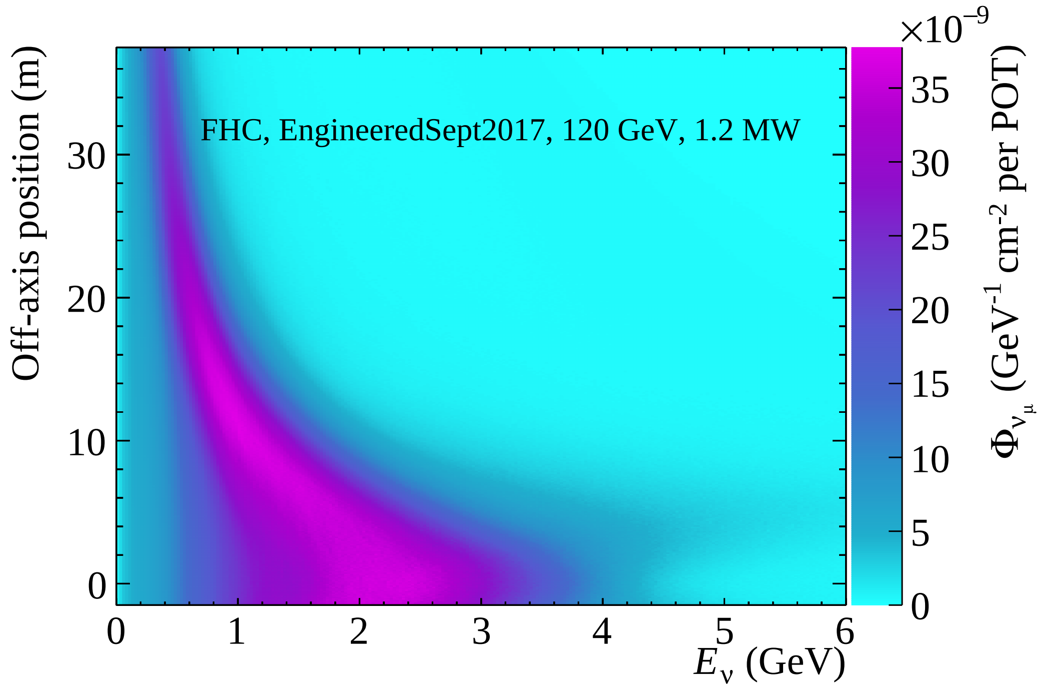

Figure 3: The predicted neutrino-mode muon neutrino energy spectra as a function of off-axis position. The effect of the off-axis position on the pion-parent peak can be clearly seen.

determining the response to parameter variations, `PPFX` [7], was not compatible with the `g4lbne` version that was used. The impact of hadronization uncertainties will be studied when this is resolved.

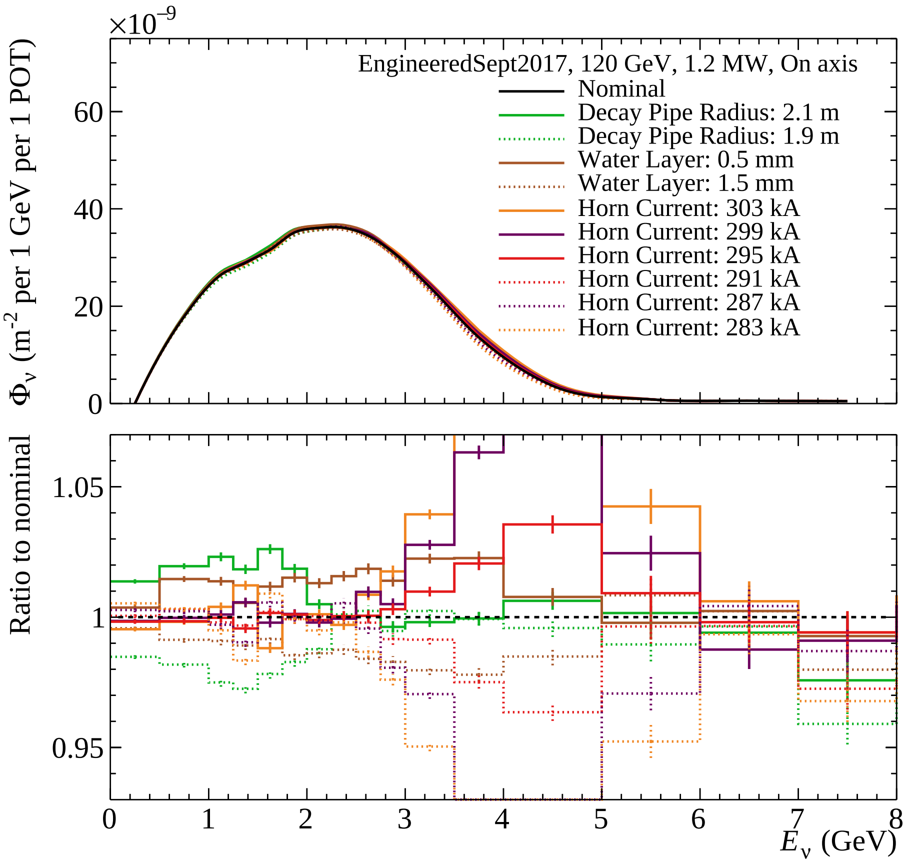

Figure 4: The response of the FHC muon neutrino spectra on-axis, to variations of the decay pipe radius, horn current, or horn cooling water layer thickness. The fractional variation to the spectra is shown in the bottom panel.

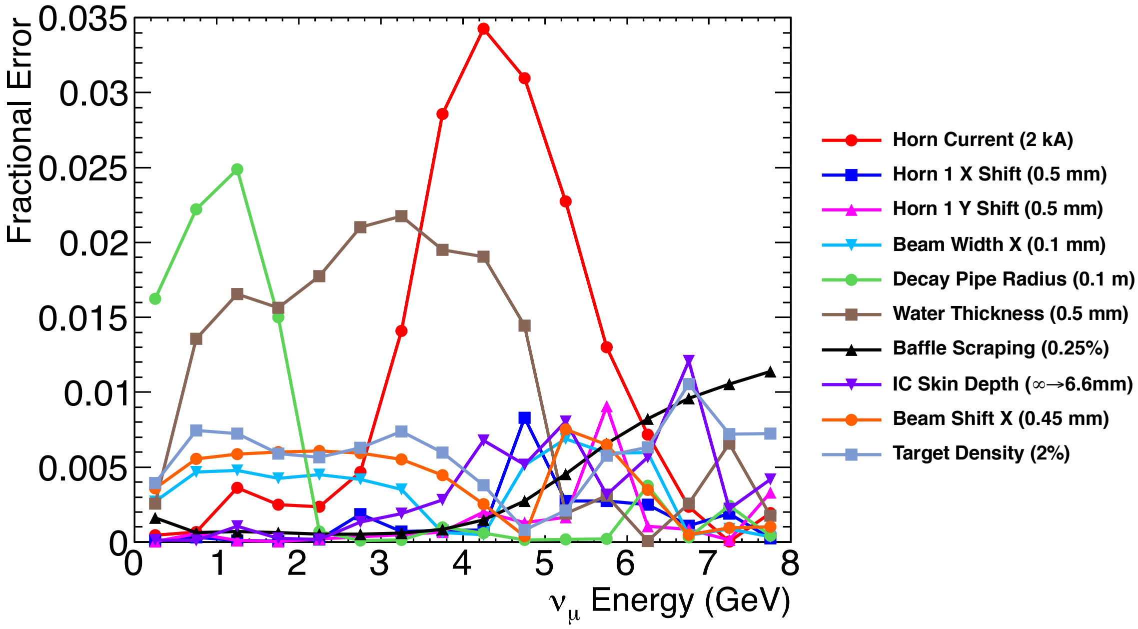

Figure 5: The fractional focussing uncertainties calculated for the near detector flux in Ref. [12]. This study was performed with an un-optimized version of the DUNE beam, but the results of the updated study, presented in Ref. [10], are qualitatively similar.

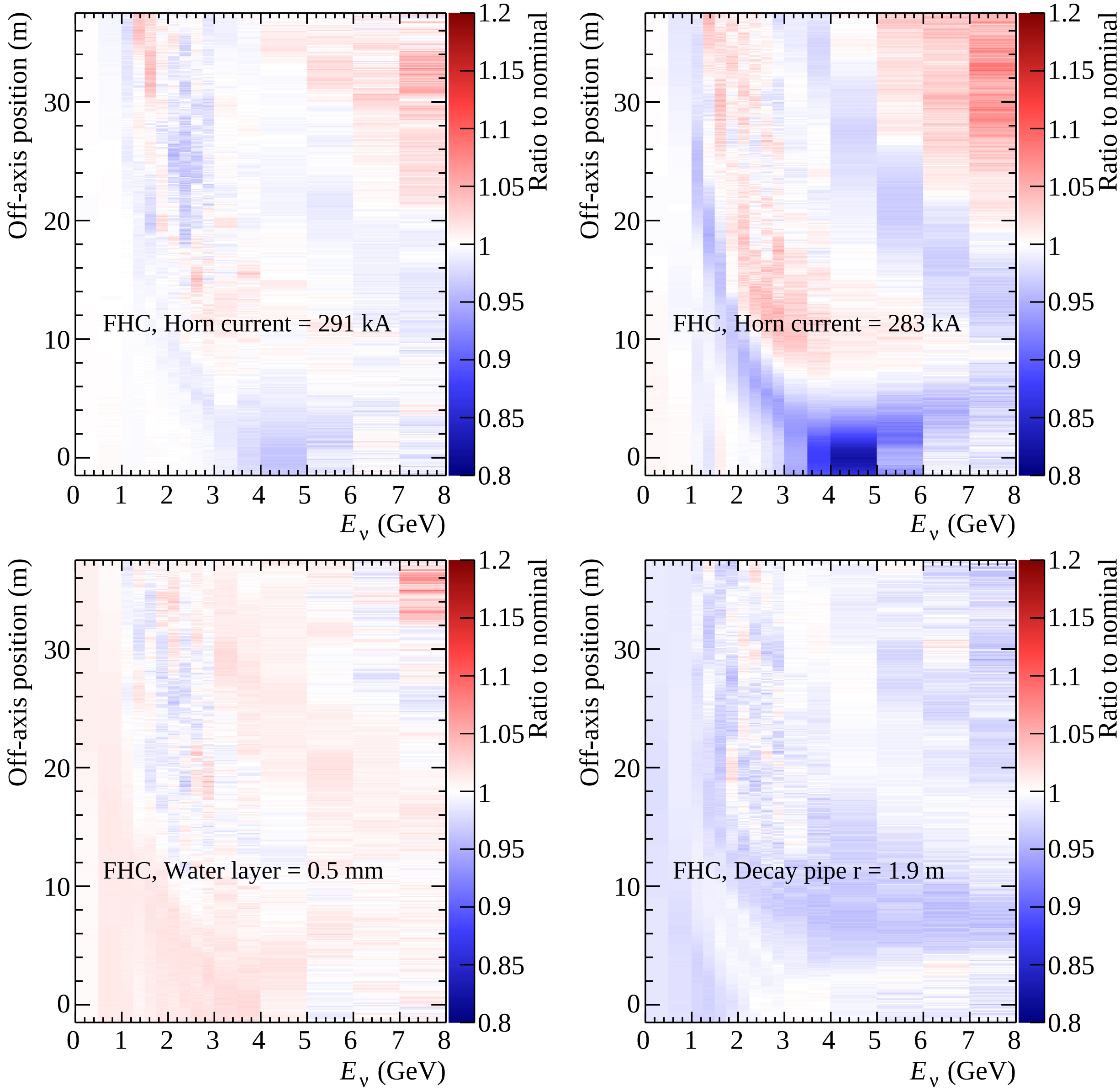

Figure 6: Off axis angle vs. E_ν projections of the impact of a few sources of uncertainties on the flux. The ratio to the nominal flux prediction is shown for variations of horn current (291 kA, -1σ, top right: 287kA, -5σ), water layer thickness (bottom left: 0.5mm) and decay pipe radius (bottom right: 1.9m)

2.2 Gaussian flux fits

Off-axis fluxes can be combined to produce Gaussian neutrino energy spectra with a well defined mean and standard deviation. These monochromatic fluxes can be used to better understand the combined effects of neutrino-nucleus scattering and detector response. Ultimately, these Gaussian flux fits are of less importance to the DUNE oscillation analysis than the oscillated flux fits, which are described in the next subsection and work quite a bit better, but they are useful to demonstrate how the information from many off-axis measurements can be used together to constrain incident neutrino energy.

The linearly combined fluxes (Φ_{LC}) are defined as:

$$\Phi_{LC}(E_\nu) = \sum_{i=0}^{N_{OA}} c_i \phi_i(E_\nu)\,, \tag{1}$$

where ϕ_i are the N_{OA} off-axis fluxes used. The coefficients c_i are found by minimizing the following figure of merit:

$$FOM = \sum_{E_\nu \text{ bins}} \frac{\left(f(E_\nu) - \Phi_{LC}(E_\nu)\right)^2}{A + B \times f^2(E_\nu)}\,, \tag{2}$$

with $f(E_\nu)$ being the target function (*e.g.,* a Gaussian function) and A and B tunable parameters.

The fits can be regularized by adding the following terms to the figure of merit:

$$\sum_{i=1}^{N_{OA}} \frac{\left(c_i - c_{i-1}\right)^2}{K}\,, \tag{3}$$

where the parameter K determines the regularization strength. These regularization terms suppress large variations in adjacent coefficients and also keep coefficients from becoming very large, which degrades the statistical precision in the combined flux.

Examples of linearly combined DUNE near detector off-axis fluxes targeting Gaussian distributions with means ranging from 0.5 GeV to 3 GeV and standard deviations of 10% can be seen in Figure 7, together with the effect of systematic variations of the decay pipe radius, horn current and horn cooling water layer thickness, as described in § 2.1.1.

Good fits are obtained across the range, with the exception of the fits with means around 2 and 2.5 GeV where a significant tail develops on the high energy side. This feature is under investigation at the time of writing and it is still unclear if it can be resolved by a better combination of the fit parameters, or if it is intrinsic to the DUNE beam, for example, due to neutrinos originating from kaon parents.

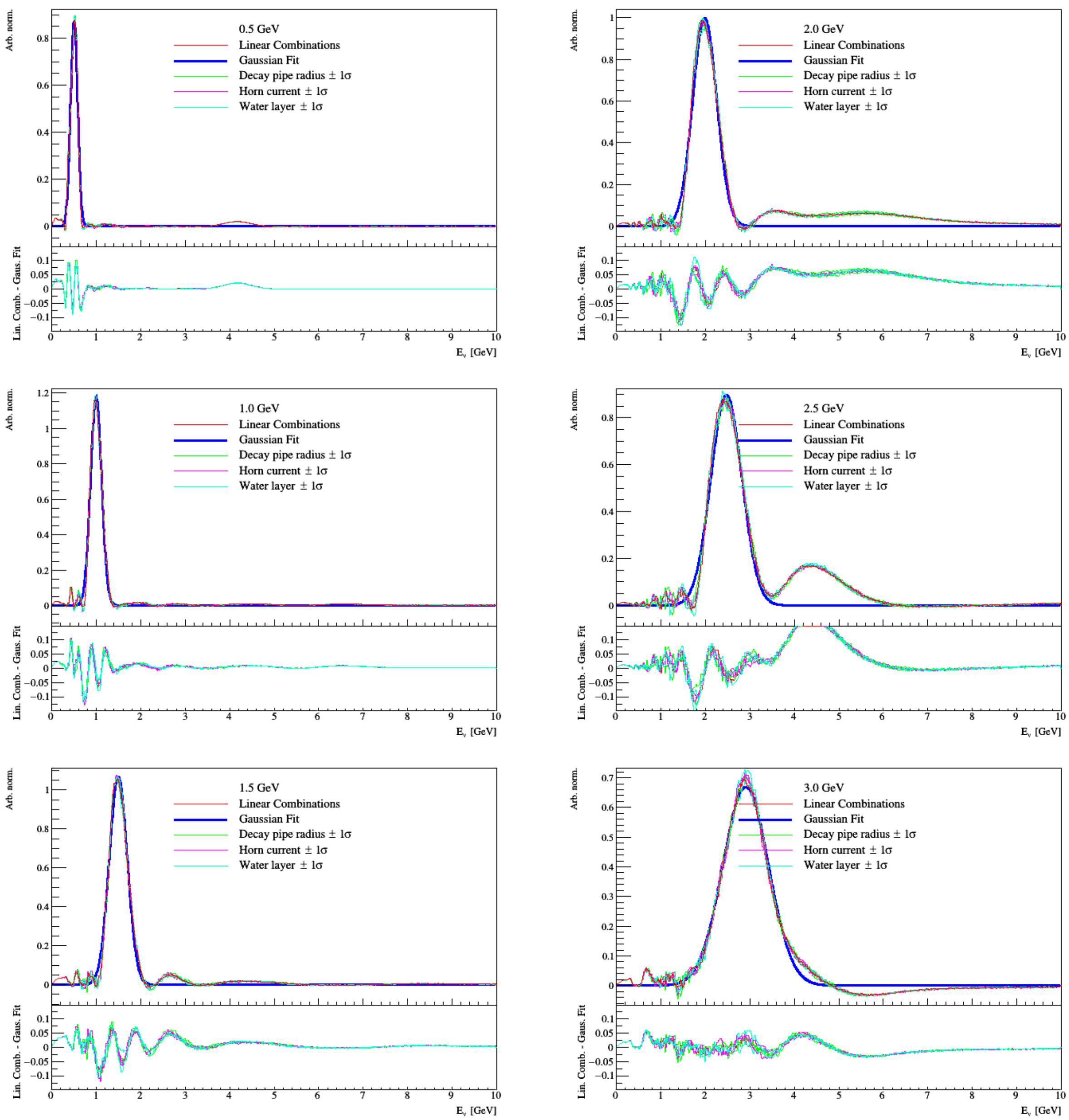

Figure 7: Linear combinations of off-axis fluxes giving Gaussian spectra with means ranging from 0.5 to 3 GeV and 10% standard deviations. The linearly combined flux obtained with the nominal beam MC is shown in red, with a Gaussian fit shown in blue. Systematic effects due to 1 σ variations of the decay pipe radius (green), horn current (magenta) and horn cooling water layer thickness (teal) are shown.

2.3 Oscillated flux fits

The linear combinations technique can be directly applied to oscillation analyses by using as a target function the far-detector oscillated flux prediction for a given set of oscillation parameters. Far detector data can then be directly compared to linearly combined near detector data to infer oscillation parameters with minimal model dependence.

Examples of linear combinations giving ν_μ oscillated spectra for maximal and non-maximal ($\sin^2\theta_{23} = 0.65$) mixing, at three points in Δm^2_{32} (2.2, 2.5 and $2.8 \times 10^{-3}\text{eV}^2$) are shown in Figure 8. The oscillation parameters were chosen to span the range of currently allowed values, assuming symmetry in $\sin^2\theta_{23}$ about 0.5.

It is particularly important that the linearly combined predictions agree well with the far detector expectation around the oscillation maxima as this is where feed-down effects due to mis-modelling can have large effects. It is expected that the linearly combined fluxes might not fully describe the very low end of the spectrum as well as part of the high energy tails. These shortcomings in the linearly combined fluxes can be corrected with model-dependent predictions, on which conventional analyses solely rely.

The oscillated spectrum fits given here show good agreement around the first and second oscillation maxima for the full range of oscillation parameters. In addition, the systematic variations of beam simulation parameters have a small effect on the oscillated spectra predictions.

It is also worth noting that while spurious features arise (with the current fitting scheme) in some of the Gaussian fits described in § 2.2, that is not the case in the oscillated spectrum fits shown here, with the exception of the very low energy region of the spectrum where the oscillation pattern becomes very rapid. One possible explanation for this is that the oscillated spectra contain smoothly falling tails which are not too dissimilar from the features in the fluxes making up the combinations, while the Gaussian target functions require the linear combinations to exactly cancel out for a wide range of E_ν, which might be difficult to do without degrading the agreement in the Gaussian peak. For the purposes of an oscillation analysis with DUNE-PRISM, only the oscillated spectrum fits shown here would be directly used.

While not shown here, this technique described here can also be applied to appearance analysis, by producing linear combinations of off-axis fluxes that mock up the energy spectrum for ν_e's appearing at the far detector under given oscillation parameters.

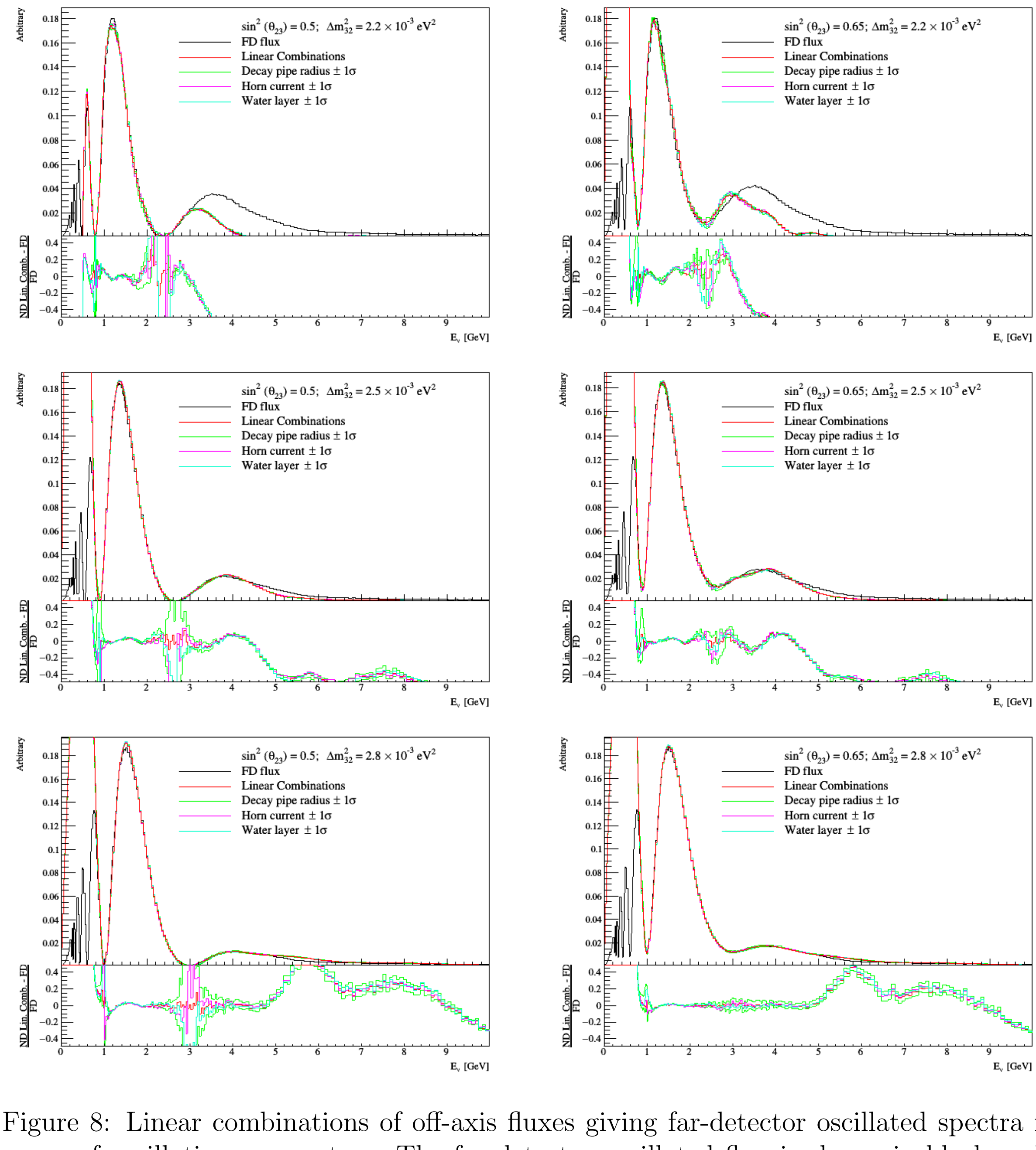

Figure 8: Linear combinations of off-axis fluxes giving far-detector oscillated spectra for a range of oscillation parameters. The far detector oscillated flux is shown in black and the linearly combined flux obtained with the nominal beam MC is shown in red. Systematic effects due to 1 σ variations of the decay pipe radius (green), horn current (magenta) and horn cooling water layer thickness (teal) are shown.

3 Sensitivity to Horn Positions and Currents

A study was done to determine the degree to which the flux spectra at different off-axis angles are sensitive to changes in horn positions or currents. The study used the 80 GeV optimized flux along with reweighting to examine the flux at different angles for changes in the horn parameters (*c.f.* § 2.1.1). The results showed the changes in the flux to be quite small (<2%) as a function of neutrino energy bins and off-axis angles for movements or rotations of the horns within the range of typical errors expected. Similarly, changes in the horn current within the expected range caused negligible changes in the flux.

Shifts or tilts of horn 1 or horn 2 by large amounts (3 mm) induced observable changes in the flux approaching 5% at a few to 10 mrad off-axis, as shown for the 3-.35 GeV neutrino energy bin in Figs. 9 and 10[3]. Similar shifts in the position or tilt in horn 3 (the most downstream horn) induced no significant changes in the flux as seen in Fig. 11. Large changes in the horn current of a few kA caused changes in the flux of a few percent that were relatively flat as a function of off-axis angle up to 10 mrad. Fig. 12 shows the change in the flux between 3.5 and 4 GeV as a function of the current shift and off-axis angle. At larger off-axis angles the flux proved to be insensitive even to these large changes in the current.

The primary conclusion of the horn error study is that the error in off-axis fluxes induced by the expected uncertainties in horn position and current parameters should contribute no more to the error budget than they do for the on-axis flux. A secondary conclusion is that larger than expected shifts in the horn positions (such as seen in NuMI) or current might induce significant changes in the flux at off-axis angles, particularly if the unexpected change is a shift in horn 1 or horn 2. In such a situation, the pattern of the change in the flux at off-axis angles might be a valuable tool in diagnosing the changing horn parameter.

[3] It is worth noting that these shifts are six times larger than the latest quoted tolerances from the beam group, as reproduced in Table 1

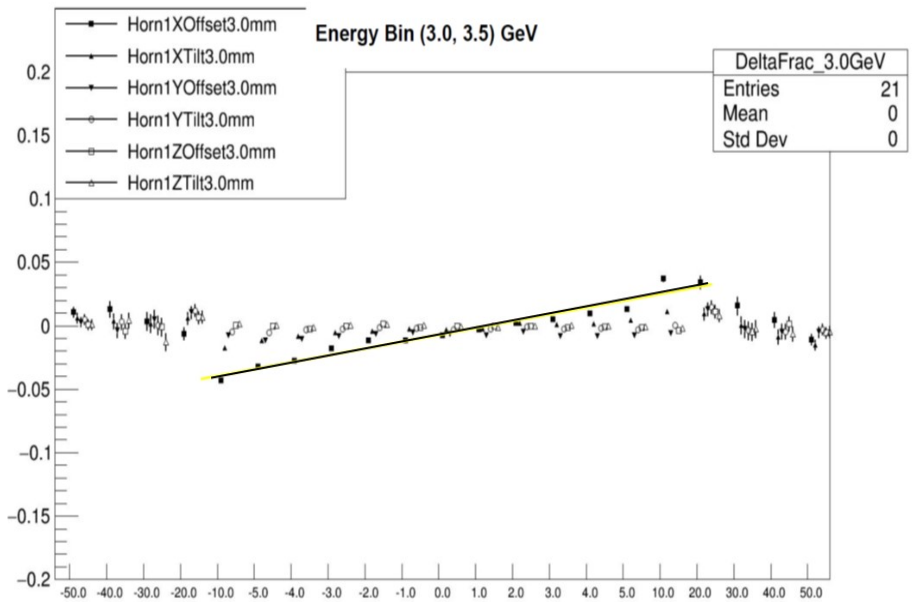

Figure 9: Relative change in flux as a function of off axis angle (in mrad) in the 3-3.5 GeV bin of neutrino energy for shifts and tilts of horn 1.

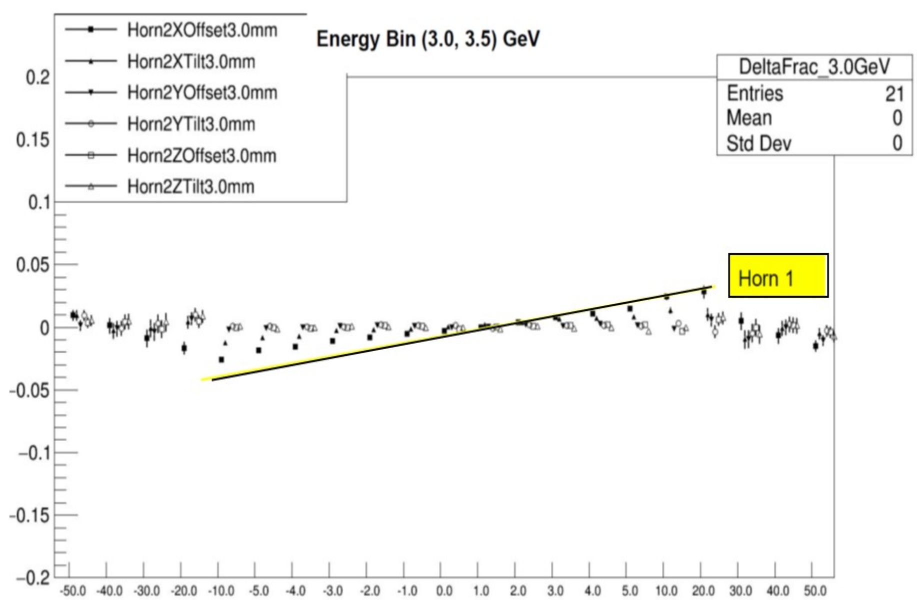

Figure 10: Relative change in flux as a function of off axis angle (in mrad) in the 3-3.5 GeV bin of neutrino energy for shifts and tilts of horn 2.

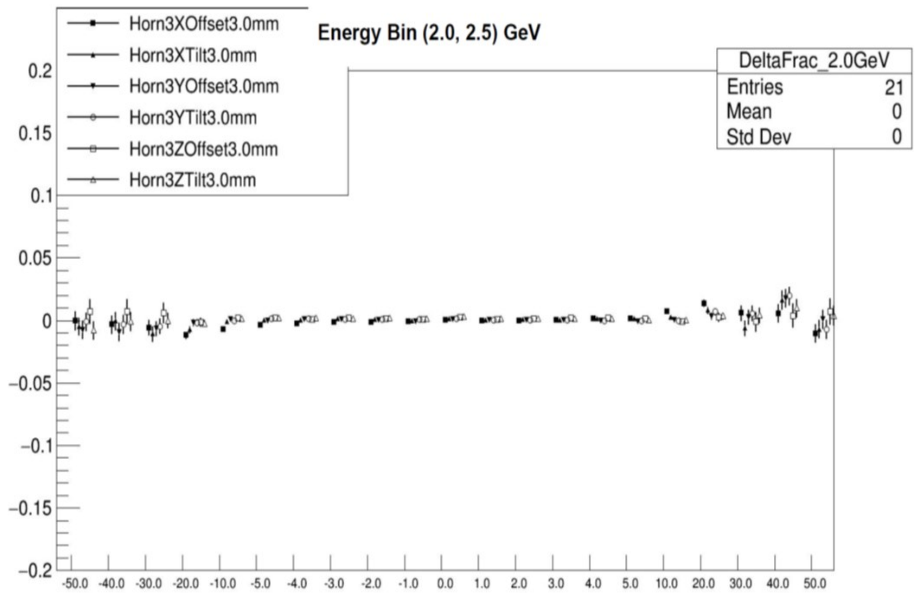

Figure 11: Relative change in flux as a function of off axis angle (in mrad) in the 2-2.5 GeV bin of neutrino energy for shifts and tilts of horn 3.

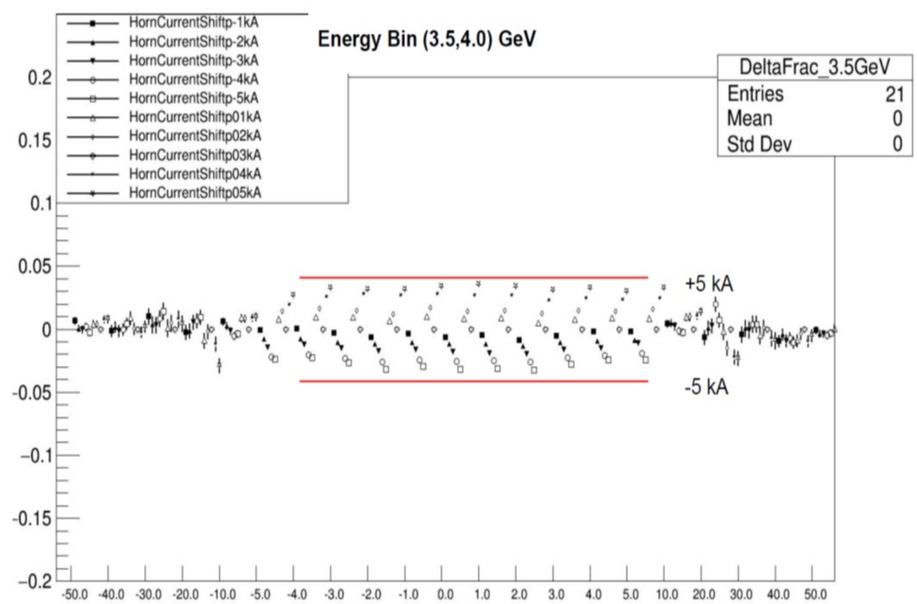

Figure 12: Relative change in flux as a function of off axis angle (in mrad) in the 3.5-4 GeV bin of neutrino energy for changes in the horn current of up to 5 kA.

4 Simple detector simulations and selected samples of contained hadronic showers

4.1 The detector simulation

To simulate the behavior of a DUNE-PRISM detector, GENIE events were generated—using the full `g4lbne` beam simulation introduced in § 2.1—in a large block of Liquid Argon 39 m(W/$\vec{x}$) $\times$ 5 m(L/$\vec{z}$) $\times$ 3 m(H/$\vec{y}$) cuboid of liquid argon. The event rate is shown as a function of off-axis position in Figure 13. After this, a set of 12 off-axis positions, or detector "stops", and one on-axis position were used to place 4 m(W) $\times$ 5 m(L) $\times$ 3 m(H) analysis volumes. A 0.5 m veto volume was applied on each side of the 'detector' region. Events that fell within the 3 m(W) $\times$ 4 m(L) $\times$ 2 m(H) fiducial volume (FV) of a stop were kept for later analysis (*c.f.* Appendix: A).

The final state particles for each selected interaction were then propagated through the liquid argon volume by a `GEANT4` simulation[4] to simulated realistic energy deposits throughout the block of Argon. These deposits were further analysed to build samples of simulated events that produced well-contained final state hadronic systems, as well as a contained muon and exiting muon sample.

[4]Many thanks to Daniel Dwyer for his work on developing his argon Box python tool, which was the basis of the GEANT4 simulation.

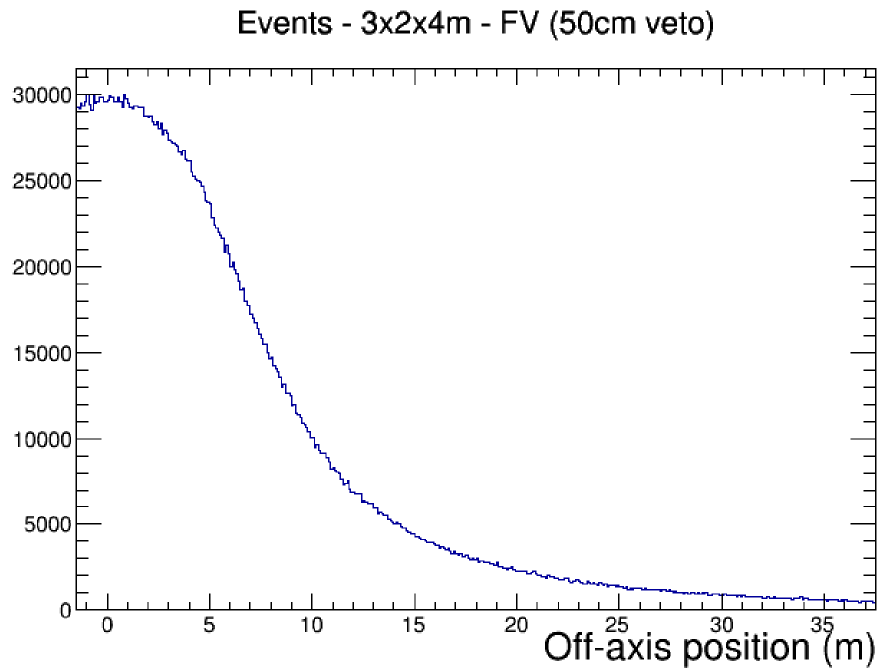

Figure 13: The distribution of ν_μ charged-current neutrino interactions occurring within the FV of a DUNE-PRISM detector stop, as predicted by a GENIE simulation. With 13 stops, the FV of the detection region at a given stop is contiguous with the neighbouring two stops.

4.2 Final state muon selection

In the case of charged-current interactions (CC), the final state muon was tracked through the volume of the liquid argon block. The final position and momenta of muons exiting, or stopping within, the detector volume that contained the original interaction were recorded—*N.B.* events with muons that stop within the veto region were kept. The efficiency for containing muons in the interactions shown in Figure 13 is presented in Figure 14a. The features seen at the edges of each fiducial volume ($-1.5\,\mathrm{m}, 1.5\,\mathrm{m}, 4.5\,\mathrm{m}$, *etc.*. . .) arise because of the lower phase space for muons produced in neutrino interactions near the edge of a detector volume to stop within the same volume. The efficiency for events producing a final state muon with more that exits the initial detection volume including veto region, with more than 50 MeV, of kinetic energy is shown in Figure 14b. Interactions that occur near the edge of a fiducial region produce muons that are more likely to exit the detector volume with sufficient kinetic energy that those occuring in the centre of a detector stop. This gives rise to the structure seen in Figure 14b.

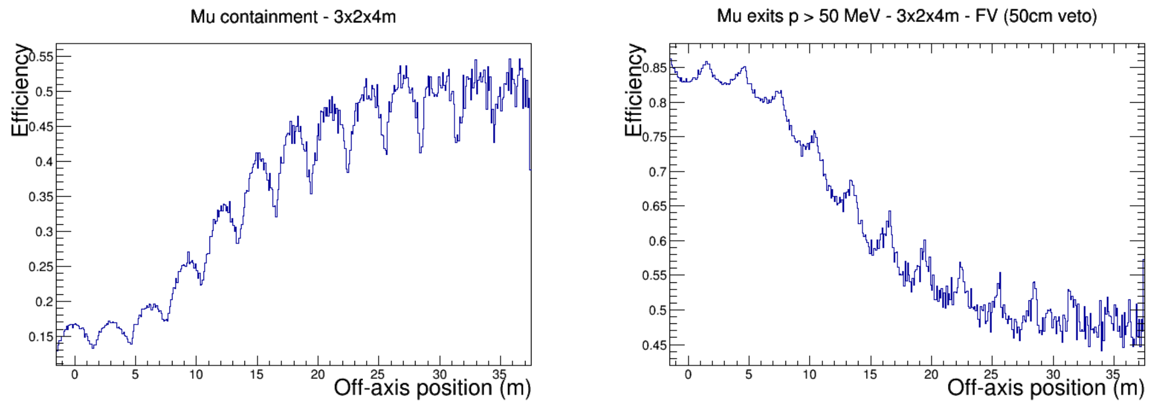

(a) Off-axis efficiency for a stopping muon

(b) Off-axis efficiency for an exiting muon

Figure 14: The efficiency for the two muon event selection: (a) muons that stopped within the same detector analysis volume in which they were produced, and (b) muons that exit the detector analysis volume with more than 50 MeV of kinetic energy. The efficiency for containing muons that are produced near the edge of detection region is lower than in the centre; the opposite is true when considering the probability that muons exit a given volume.

4.3 Hadronic system containment

To accurately characterise estimate the neutrino energy for a given selected interaction, both the leptonic and hadronic systems must be sampled. A sample of events with well-contained hadronic deposits were selected by enforcing that no more than 10 MeV[5] of energy was deposited within the veto region surrounding the fiducial region at each stop. Such a selection allows an increased confidence that the energy deposited by final state particles leaving the neutrino interaction were well sampled. In the event selection, deposits that were made outside of the veto region—*i.e* outside of the 'active' region of each detector stop—were not 'visible' to the selection. Thus events may be selected that appeared fully contained, but were not according to the MC truth, such as events that contain a neutral pion that left the detector region before decaying.

While there are many illuminating kinematic projections of the selection efficiency, it is interesting to check that the hadronic containment for similar event topologies doesn't vary as a function of off-axis position. The elasticity, $\mathrm{E} = 1 - y$, where $y = \omega/E_{\nu}$, characterises the fraction of the neutrino energy that remains in the leptonic system. It can be seen from Figure 16 that even though the neutrino energy spectra varies significantly as a function of off-axis angle, the efficiency for containing the hadronic system only depends upon the fractional energy transfer to the hadronic system—as should be expected.

[5]The choice of 10 MeV is somewhat arbitrary, but as seen in Appendix: B, the selection efficiency does not change significantly between 10 MeV and 20 MeV cuts.

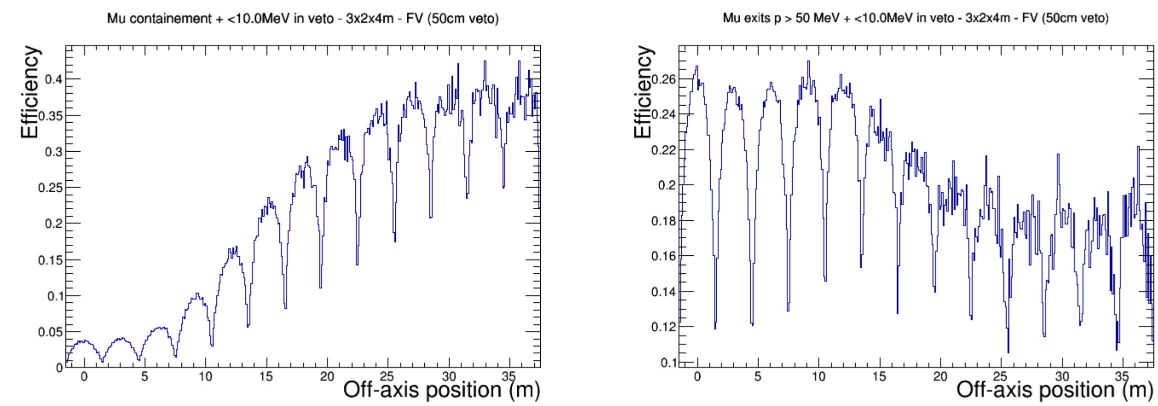

(a) Stopping muon with contained hadronic system (b) Exiting muon with contained hadronic system

Figure 15: The selection efficiency for contained hadronic events for the two muon selections shown in Figure 14. The shape of the efficiency is dominated by the low probability for interactions occurring near a veto region to pass the hadronic containment selection—as should be expected.

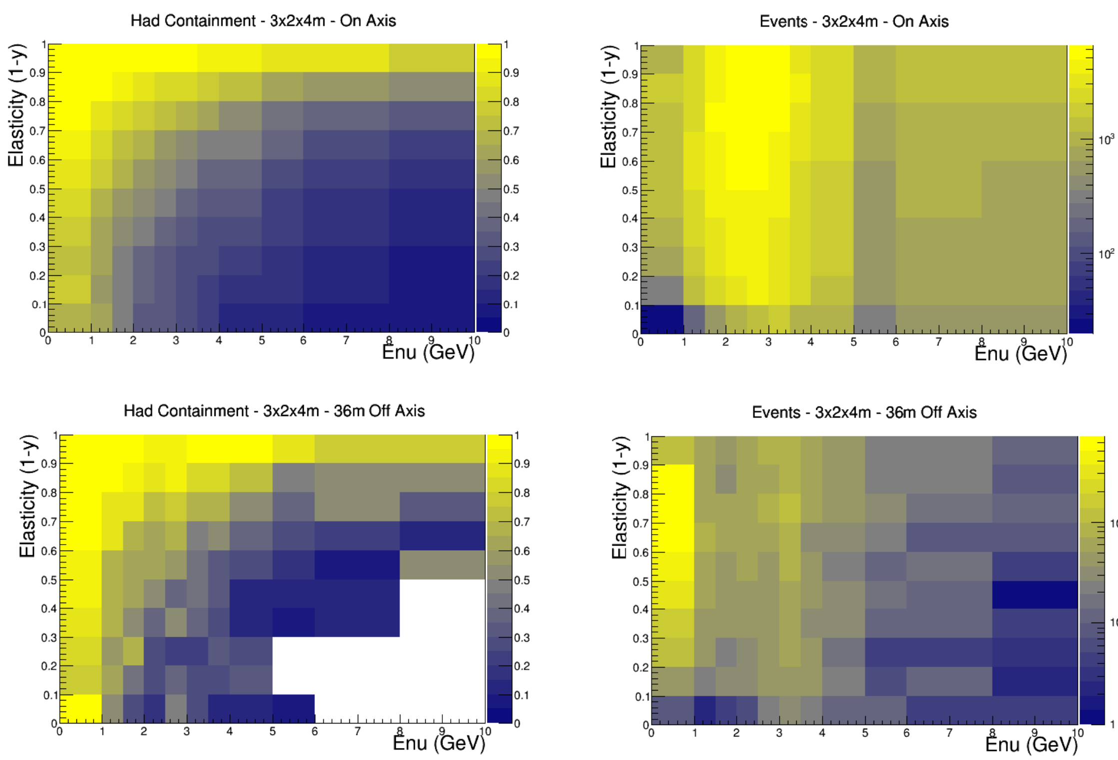

Figure 16: The probability for hadronic containment (left) and the overall simulated event rate (right) for the on-axis (top) and 36 m off-axis (bottom) positions. The containment efficiency shape is qualitatively the same for both detector stops. *N.B.* The muon selections described in § 4.2 are not applied in these distributions.

5 Event rate predictions

The predictions presented in this section were made using a full `g4lbne` + `GENIE` + `GEANT4` simulation, with event selections applied to collections of energy deposits simulated by `GEANT4`, where applicable, full MC truth information was used. The hadronic energy cut was applied to all simulated events—surviving simulated interactions are then further selected into muon-contained and muon-exiting samples. The cuts are described in more detail in § 4. The contents of the two samples for a full year of FHC running (1.1×10^{21}) are shown in Table 2. The predictions are POT-scaled from the results of the study presented in § 4 to an example year-long run plan that takes 50% of the available POT on axis and spreads the remaining beam time equally among the twelve off axis stops. In addition to the selected muon neutrino event rate, the selected wrong-sign fraction and the selected intrinsic electron neutrino and neutral current rates are presented. While the rates off axis are lower than those predicted on axis, a significant number of interactions will be recorded. It is worth noting that the hadronic containment cut may be overly strict for practical analyses and as such these rate predictions may be considered somewhat conservative. It is likely that the muon-exiting sample would be considered the signal sample in an oscillation analysis. Such an analysis would most likely require a downstream detector capable of sign-selection.

Offset	10^{19}POT	CCInc							NCInc
		μ contained			μ exit, $T_\mu^{\text{exit}} > 50$MeV			ν_e	ν_μ
		ν_μ	$\epsilon_{\nu_\mu,\text{CC}}$	$\bar{\nu}_\mu/\nu_\mu$	ν_μ	$\epsilon_{\nu_\mu,\text{CC}}$	$\bar{\nu}_\mu/\nu_\mu$		
0 m	55	6.6E5	3%	1%	5.3E6	22%	3%	6.2E4	1.8E6
3 m	4.58	5.5E4	3%	1%	4.1E5	22%	3%	5.0E3	1.4E5
6 m	4.58	5.8E4	4%	1%	3.0E5	22%	4%	4.3E3	1.1E5
9 m	4.58	6.0E4	7%	2%	1.9E5	22%	4%	3.4E3	7.5E4
12 m	4.58	5.9E4	12%	3%	1.1E5	22%	5%	2.5E3	5.2E4
15 m	4.58	5.4E4	18%	3%	6.2E4	20%	6%	2.2E3	3.7E4
18 m	4.58	4.6E4	22%	4%	3.8E4	18%	8%	1.7E3	2.7E4
21 m	4.58	3.9E4	27%	5%	2.5E4	17%	9%	1.4E3	2.1E4
24 m	4.58	3.1E4	30%	6%	1.7E4	16%	9%	1.2E3	1.6E4
27 m	4.58	2.6E4	32%	7%	1.2E4	15%	10%	9.8E2	1.3E4
30 m	4.58	2.1E4	33%	7%	9.6E3	16%	12%	8.3E2	1.0E4
33 m	4.58	1.7E4	35%	8%	7.5E3	15%	13%	7.6E2	8.3E3
36 m	4.58	1.2E4	35%	8%	6.1E3	16%	15%	6.7E2	6.6E3
Totals		ν_μ	—	$\bar{\nu}_\mu$	ν_μ	—	$\bar{\nu}_\mu$	ν_e	ν_μ
All	110	1.1E6	—	1.6E4	6.5E6	—	2.2E5	8.7E4	2.3E6

Table 2: The selected event rates for a year-long, neutrino-mode run plan, as predicted by the study presented in § 4. The wrong sign fraction, intrinsic electron neutrino and neutral current event rates are also shown. In all cases, the hadronic containment cut is applied, and the (anti-)muon neutrino events are separated into two samples depending on the containment topology of the final state muon.

6 Fake Data Bias Studies with CAFAna

The information provided by DUNE-PRISM can be used in 2 important ways:

1. Off-axis measurements can be used to identify problems in the neutrino interaction model. This goal can likely be achieved with measurements at just a few off-axis locations.

2. Off-axis measurements can be used to overcome issues in the neutrino interaction model by providing far detector predictions that are largely based on near detector data, rather than the model. This goal requires measurements across most or all of the off-axis range from 0° to about 3°.

This section provides an example of the first of these two uses of DUNE-PRISM measurements. A fake dataset has been produced in which 20% of the pion kinetic energy is instead carried by neutrons (this loss in pion energy could be due to detector inefficiency, modeling of the presumed pion spectrum, and/or final state interactions). This data is fit with the standard DUNE near detector neutrino interaction model that does not have a parameter for modifying just the pion kinetic energy (although neutrino energy scale and resolution can be modified in the fit).

The framework we use to do the oscillation fit is CAFAna, which is the oscillation fit framework used in NOvA experiment. Note that this is the version of CAFAna that has been used thus far for DUNE, and is not exactly what NOvA is using. The near and far detector samples we use are from the near detector task force (NDTF) [9]. The near detector is assumed to be a fine grain tracker and the far detector is a liquid argon TPC. We assume 7 years data taking time and a 40 kton FD and a 100 ton ND. The fitting sample includes ν_μ, $\overline{\nu_\mu}$, ν_e and $\overline{\nu_e}$ in FHC and RHC modes. The systematics included are 32 cross section parameters from the DUNE Near Detector Task Force studies [9], 5 major flux parameters, energy scale and energy resolution. The list of all the systematics parameters are shown in Table 3. The cross section systematic parameters are all normalizations for a particular interaction process and Q^2 or E_ν bin. Correlations were assessed by the GENIE group, by propagating a series of physics effects into the empirical parameters. For example, variations on the axial and vector form factors are used to propagated to correlations between QE normalizations. Some uncertainties were assessed by looking at overlay plots to available data. Unlike the normalization parameters, the FSI parameters are non-linear based on long-standing conventional GENIE uncertainties.

The fake data assumes that 20% of the charged pion kinetic energy predicted by GENIE is instead carried away by unobserved neutrons. We take the DUNE flux from official simulation and GENIE is used to generate the neutrino interactions. After that, we take out 20% of the charged pion kinetic energy, then in order to obtain a ratio spectrum, the fake data sample is divided by the nominal sample in true neutrino energy. That ratio spectrum is used to generate the fake data based on the NDTF samples. The nominal MC is fitted to the fake data with floating of the systematic uncertainties and oscillation parameters. Figure 17 shows the resulting best-fit contours on the ($\sin^2\theta_{23}$ vs. Δm^2_{23}) and (δ vs. $\sin^2 2\theta_{13}$) planes. The contours correspond to 68%, 90% and 95% confidence levels. The nominal value for those parameters are $\sin^2\theta_{23}$=0.5, Δm^2_{23}=2.45x10^{-3} eV^2, Δ=1.5π and $\sin^2 2\theta_{13}$=0.085.

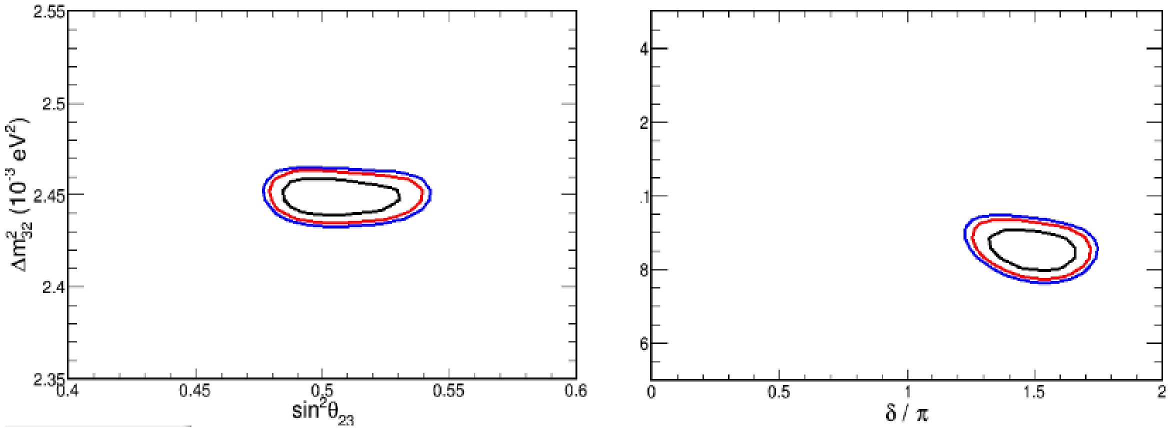

Figure 17: Nominal fitting contours on ($\sin^2\theta_{23}$ vs. Δm^2_{23}) and (δ vs. $\sin^2 2\theta_{13}$) planes.

For the fake data of 20% missing charged pion energy, the fitted contours are shown in Figure 18, with the same conventions as Figure 17.

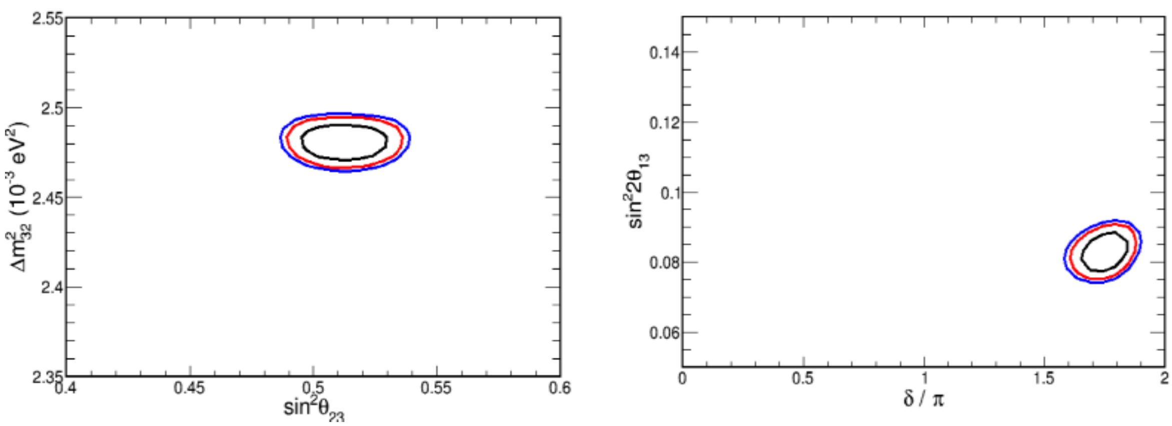

Figure 18: 20% missing charged pion energy fake data fitting contours on ($\sin^2\theta_{23}$ vs. Δm^2_{23}) and (δ vs. $\sin^2 2\theta_{13}$) planes.

The values of all four parameters are biased comparing to the nominal case, especially Δm^2_{23} and δ, in which case the biases are beyond 2 σ. In addition to the fitting contours, The fitting spectra are shown in Figure 19. From top left to bottom right are ND FHC, ND RHC, FD FHC disappearance, FD RHC disappearance, FD FHC appearance and FD RHC appearance. The nominal spectra, fake data spectra and the best fit spectra are shown.

Table 4 shows all the output systematic uncertainty parameter values. In general, the flux uncertainties are larger than cross section uncertainties, therefore, the flux systematics vary significantly to compensate the fake data shift. What is troubling about this exercise is that our near detector fits the data well so we have no indication that our oscillation fit may be biased (and it is). The χ^2 of this fit is relatively large, but a more sophisticated analysis that includes detector resolution and systematic uncertainties, as well as additional flux and cross section uncertainties, can likely produce similar results with a smaller χ^2 value.

If we have some off-axis measurements from the near detector, we can clearly see that something is wrong with the cross section model. Figure 20 shows the nominal(black), on-axis best fit(blue) and fake data(red) spectra in 30 and 45 mrad off-axis locations including both the nominal and tuned prediction based on on-axis data. Figure 21 shows the same thing but without the flux parameters since those on-axis flux parameters may not be suitable to the off-axis locations. The on-axis best fit goes up in general since it is in the low energy region of the on-axis spectrum. Nevertheless, the off-axis fake data shift to the left. So the mismatch of the fake data and on-axis best fit can be identified by these additional off-axis measurements.

Component	Magnitude	Comment
ν CCQE 1	8.2%	$Q^2 < 0.2$
ν CCQE 2	23%	$0.2 < Q^2 < 0.9$
ν CCQE 3	48%	$Q^2 > 0.9$
$\overline{\nu}$ CCQE 1	8.7%	$Q^2 < 0.2$
$\overline{\nu}$ CCQE 2	24%	$0.2 < Q^2 < 0.9$
$\overline{\nu}$ CCQE 3	40%	$Q^2 > 0.9$
ν MEC dummy	100%	
$\overline{\nu}$ MEC dummy	100%	
ν CC1π^0 1	13%	$Q^2 < 0.35$
ν CC1π^0 2	23%	$0.35 < Q^2 < 0.90$
ν CC1π^0 3	35%	$Q^2 > 0.90$
ν CC1$\pi^\pm$ 1	13%	$Q^2 < 0.30$
ν CC1$\pi^\pm$ 2	24%	$0.30 < Q^2 < 0.80$
ν CC1$\pi^\pm$ 3	40%	$Q^2 > 0.80$
$\overline{\nu}$ CC1π^0 1	16%	$Q^2 < 0.35$
$\overline{\nu}$ CC1π^0 2	27%	$0.35 < Q^2 < 0.90$
$\overline{\nu}$ CC1π^0 3	35%	$Q^2 > 0.90$
$\overline{\nu}$ CC1$\pi^\pm$ 1	16%	$Q^2 < 0.30$
$\overline{\nu}$ CC1$\pi^\pm$ 2	30%	$0.30 < Q^2 < 0.80$
$\overline{\nu}$ CC1$\pi^\pm$ 3	40%	$Q^2 > 0.80$
ν 2 π	22%	
$\overline{\nu}$ 2 π	22%	
ν DIS 1	3.5%	$E_\nu < 7.5$
ν DIS 2	3.5%	$7.5 < E_\nu < 15$
ν DIS 3	2.7%	$E_\nu > 15$
$\overline{\nu}$ DIS 1	1%	$E_\nu < 7.5$
$\overline{\nu}$ DIS 2	1.7%	$7.5 < E_\nu < 15$
$\overline{\nu}$ DIS 3	1.7%	$E_\nu > 15$
ν COH	128%	
$\overline{\nu}$ COH	134%	
ν NC	16%	
$\overline{\nu}$ NC	16%	
$\nu_e\nu_\mu$ dummy	3%	Not implemented yet
Energy scale	2%	
Energy resolution	6%	
5 major flux uncertainty	shape dependent	

Table 3: Systematic uncertainty parameters included.

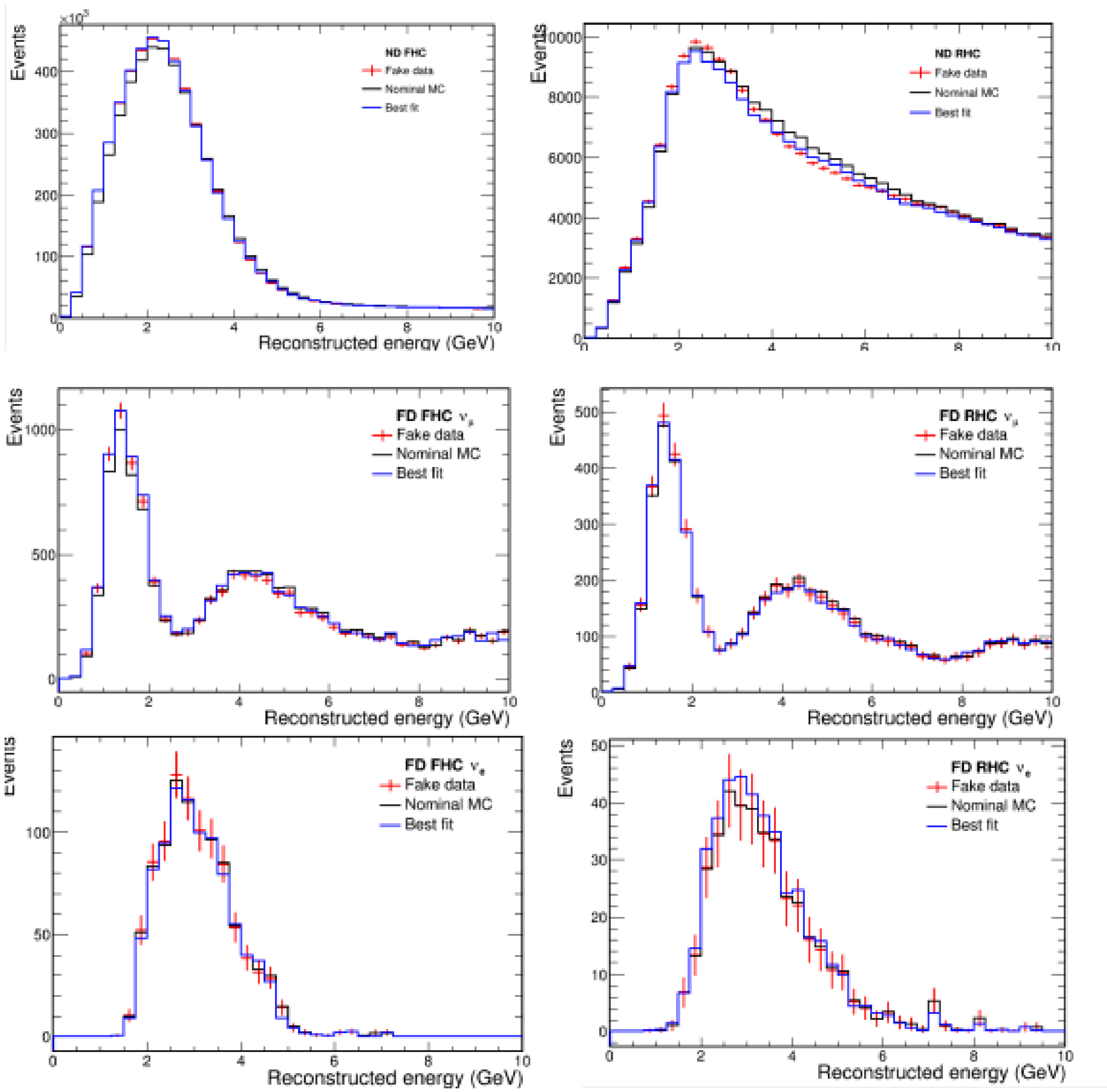

Figure 19: 20% missing charged pion energy fake data fitting spectra for ND and FD FHC and RHC. The black spectra are nominal, the red are fake data and the blue are best fit.

Systematics	Values	comments
ν CCQE 1	-0.0002	$Q^2 < 0.2$
ν CCQE 2	-5.2x10^{-5}	$0.2 < Q^2 < 0.9$
ν CCQE 3	-1.0x10^{-5}	$Q^2 > 0.9$
$\overline{\nu}$ CCQE 1	0.0003	$Q^2 < 0.2$
$\overline{\nu}$ CCQE 2	8.0x10^{-5}	$0.2 < Q^2 < 0.9$
$\overline{\nu}$ CCQE 3	5.4x10^{-6}	$Q^2 > 0.9$
ν MEC dummy	3.5x10^{-7}	
$\overline{\nu}$ MEC dummy	5.0x10^{-7}	
ν CC1π^0 1	0.0001	$Q^2 < 0.35$
ν CC1π^0 2	0.0003	$0.35 < Q^2 < 0.90$
ν CC1π^0 3	-0.0002	$Q^2 > 0.90$
ν CC1$\pi^\pm$ 1	8.7x10^{-5}	$Q^2 < 0.30$
ν CC1$\pi^\pm$ 2	-9.5x10^{-5}	$0.30 < Q^2 < 0.80$
ν CC1$\pi^\pm$ 3	0.0002	$Q^2 > 0.80$
$\overline{\nu}$ CC1π^0 1	-0.0005	$Q^2 < 0.35$
$\overline{\nu}$ CC1π^0 2	-0.0004	$0.35 < Q^2 < 0.90$
$\overline{\nu}$ CC1π^0 3	0.0002	$Q^2 > 0.90$
$\overline{\nu}$ CC1$\pi^\pm$ 1	-6.6x10^{-5}	$Q^2 < 0.30$
$\overline{\nu}$ CC1$\pi^\pm$ 2	4.4x10^{-5}	$0.30 < Q^2 < 0.80$
$\overline{\nu}$ CC1$\pi^\pm$ 3	-6.3x10^{-5}	$Q^2 > 0.80$
ν 2 π	-0.786	
$\overline{\nu}$ 2 π	-0.07	
ν DIS 1	-0.0003	$E_\nu < 7.5$
ν DIS 2	-0.0011	$7.5 < E_\nu < 15$
ν DIS 3	0.0013	$E_\nu > 15$
$\overline{\nu}$ DIS 1	4.5x10^{-5}	$E_\nu < 7.5$
$\overline{\nu}$ DIS 2	-0.004	$7.5 < E_\nu < 15$
$\overline{\nu}$ DIS 3	0.003	$E_\nu > 15$
ν COH	0.0001	
$\overline{\nu}$ COH	-0.0001	
ν NC	0.0006	
$\overline{\nu}$ NC	-0.0017	
flux 1	1.023	
flux 2	-2.354	
flux 3	3.219	
flux 4	-2.036	
flux 5	1.713	
Energy scale	-0.821	
Energy resolution	-0.044	
χ^2	749.5 (d.o.f=202)	

Table 4: Values of systematic parameters as a result of the oscillation fit using 20% missing pion energy fake data. All the nominal values are 0.

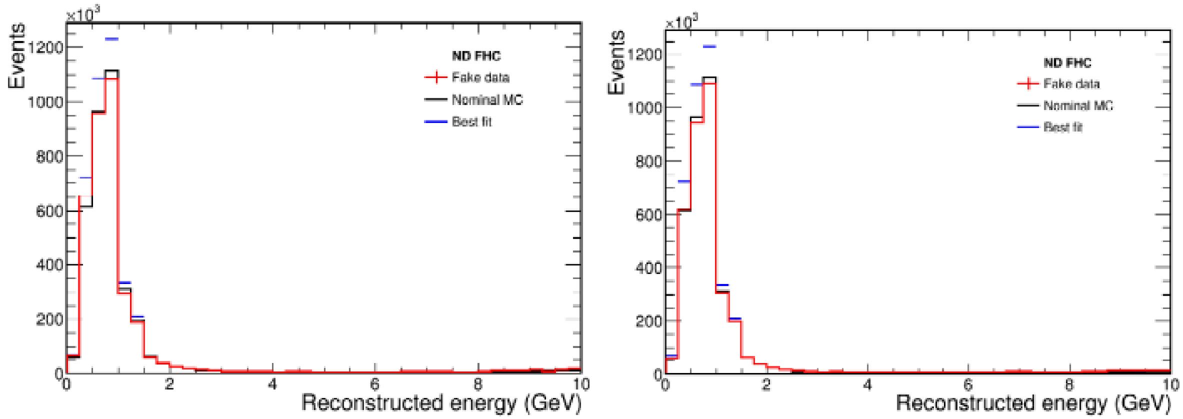

Figure 20: Comparison of on-axis best fit(blue), off-axis nominal(black) and off-axis fake data(red) spectra. Left: 30 mrad off-axis; Right: 45 mrad off-axis.

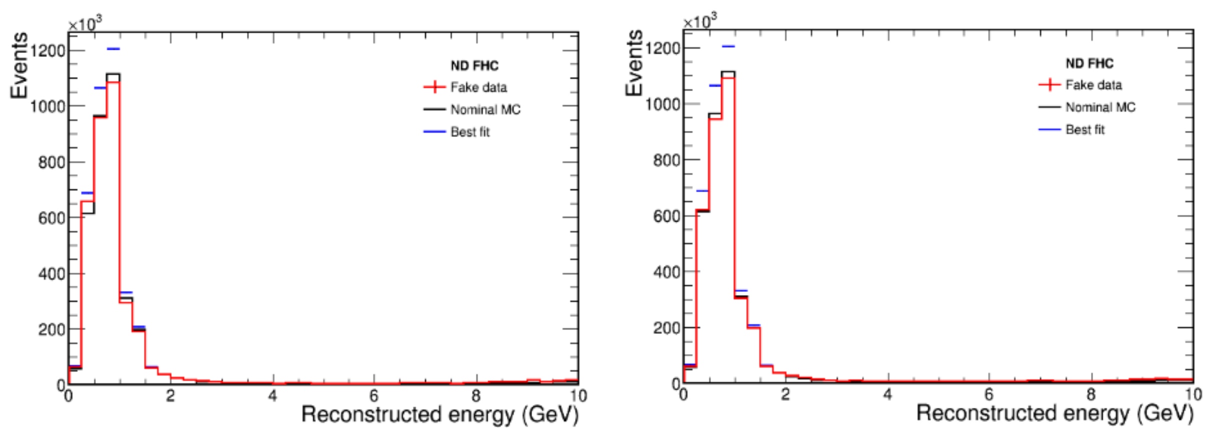

Figure 21: Without flux parameters, comparison of on-axis best fit(blue), off-axis nominal(black) and off-axis fake data(red) spectra. Left: 30 mrad off-axis; Right: 45 mrad off-axis.

7 Conclusion

The first set of DUNE-PRISM studies presented in this note demonstrate the power of off-axis measurements in addressing deficiencies in the neutrino interaction model.

1. Linear combinations of off-axis measurements can produce Gaussian energy spectra over much of the interesting range for DUNE, which allow for a direct measurement of the relationship between true and reconstructed neutrino energy. The fits in the 2-2.5 GeV region show spurious high-energy tails in the current round of fits, and we are investigating modifications to the fit regularization to mitigate their effect.

2. The linear combinations can fit the far detector oscillated spectra over nearly the entire energy range (including the 1st and 2nd oscillation maxima) for any currently allowed values of the oscillation parameters. This should allow for a data driven far detector prediction with very little model-dependent correction required.

3. The existing flux systematic errors, including focusing effects such as horn current uncertainties, have been shown to have little impact on the flux linear combinations.

4. If unexpected flux uncertainties are observed, such as the misalignment of the first or second horn, off-axis measurements can provide useful information for diagnosing the problem.

5. A sample run plan has been provided for making a set of DUNE-PRISM off-axis measurements in 1 year of forward horn current running with realistic detector efficiencies (although the effect of rock muon pileup has not yet been considered). Collecting 50% of the data taking on-axis and the other 50% of the data at 12 different off-axis positions provides >10,000 accepted events at each position, and allows for both a contained muon, and an escaping muon event selection. More detailed numbers can be produced when decisions are made regarding the number and size of side muon range detectors.

6. An initial fake data study in which 20% of the pion kinetic energy is carried away by unobserved neutrons shows that a full near/far fit using only on-axis near detector measurements can result in a reasonably good fit to the data, and still produce a biased measurement of oscillation parameters. These biases can be identified via additional off-axis measurements.

The next steps for the DUNE-PRISM analysis include a full near/far fit using a set of off-axis angle measurements, which are expected to show little sensitivity to neutrino interaction modeling in fits to various fake data samples.

A Simulation set up

The decay positions of neutrino parent partcles are shown in Figure 22. In this coordinate system the proton target is at the origin and the proton beam hits the target with an average direction $\vec{z}$.

The LBNF neutrino beamline will use a 5.8° dip angle with respect to the horizon at the target station to point the neutrino beam towards the far detector site, 1287 km away in Lead, South Dakota [13].

The near detector is situated at 575 m from the target station and is simulated as a 39 m(W) × 5 m(L) × 3 m(H) cuboid of liquid argon. The cuboid is translated by 18 m in the $-x$ direction so that the analysis can place simulated detection volumes on axis, and then at a range of off-axis positions. The near detector coordinate system origin is placed at the centre of the on-axis detection box; the `dk2nu` GENIE flux driver applies the coordinate rotation and translation between target-origin and the near detector system [8]. The `dk2nu` flux driver forces neutrino rays to pass through a user-configured flux window and then includes the calculated phase space weight in the neutrino interaction throws (*c.f.* § 2.1.1). The X/Y and Z/Y projections of the forced neutrino momenta for a sample of interactions in the near detector are shown in Figure 23. It can be seen that the rotation and translation were performed successfully as neutrinos that interact in the near detector had momentum vectors pointing in the $-y$, $+z$ direction. The spread in x momentum is due to the asymmetric off-axis extent of the simulated near detector.

The simulated interaction positions for a sample of 2×10^{19} POT-equivalent interactions is shown in Figure 24. The shadow of the flux window can be seen by the low, but non zero, interaction rate in the air outside of the liquid argon cuboid. The veto region used in the hadronic containment cuts in § 4 has been overlaid on Figure 24a. The fiducial regions at each of the detector stops used in § 4 and § 5 are overlaid in white on Figure 24b.

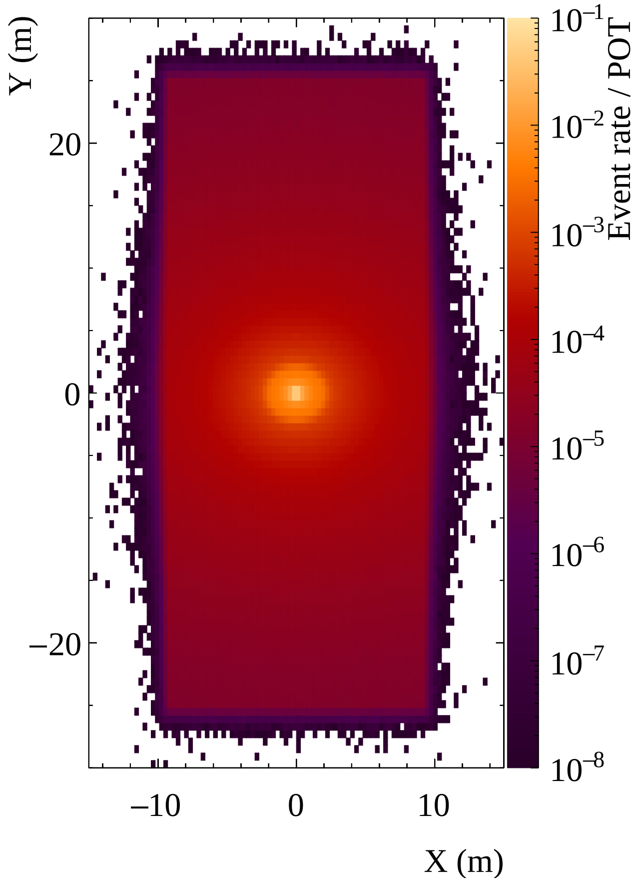

(a) X/Y decay parent position projection

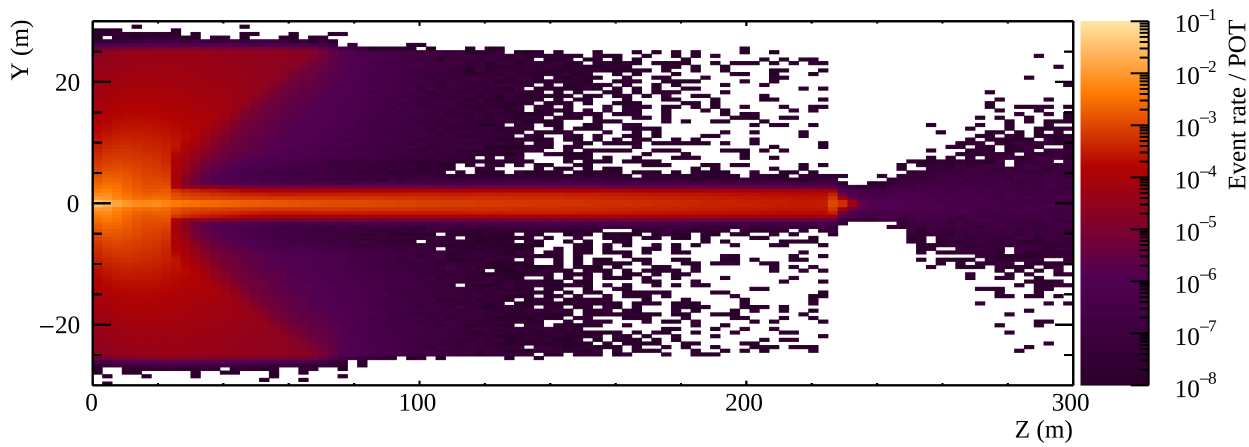

(b) Z/Y decay parent position projection

Figure 22: X/Y (a) and Z/Y (b) projections of the position in target-origin coordinates of neutrino parent particle decay positions. In these coordinates the target, situated inside horn 1, is at the origin.

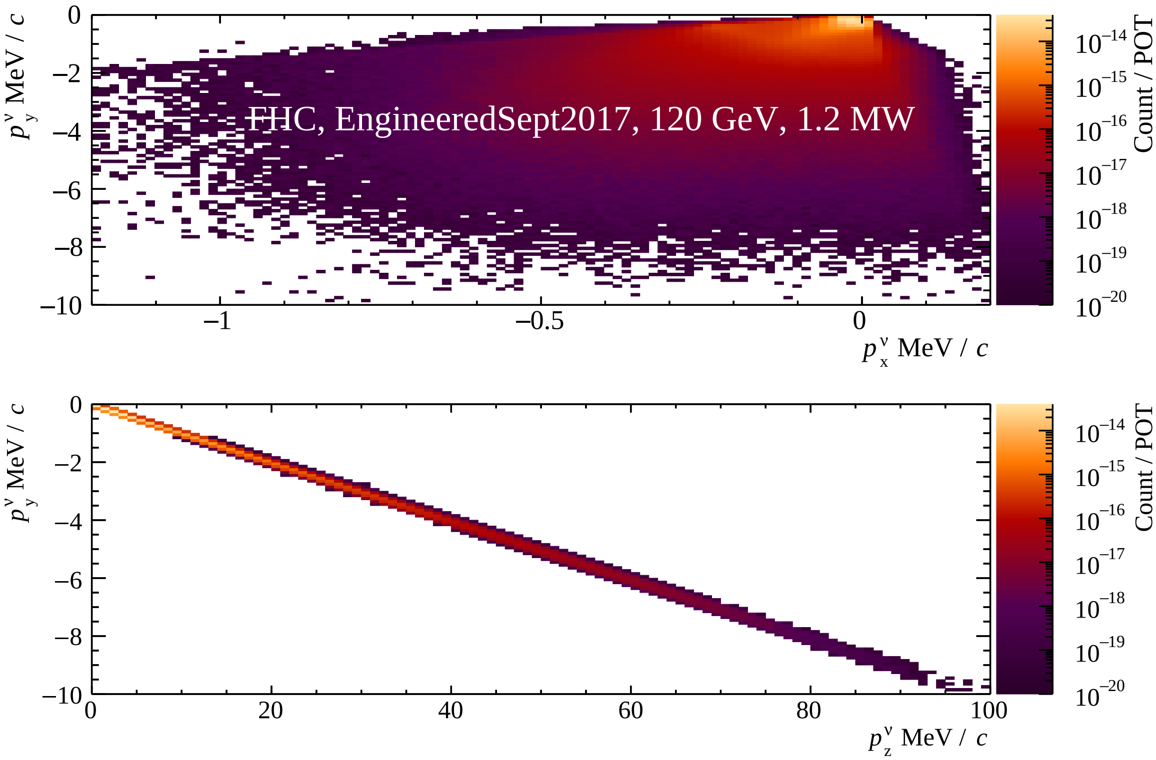

Figure 23: The X/Y (a) and Z/Y (b) projections of the neutrino momentum for neutrinos that interacted in the GENIE near detector simulation. The effect of the coordinate transformation from target-origin to near detector coordinates can be seen—neutrinos that interact in the near detector had to travel in approximately the $-y$, $+z$ direction.

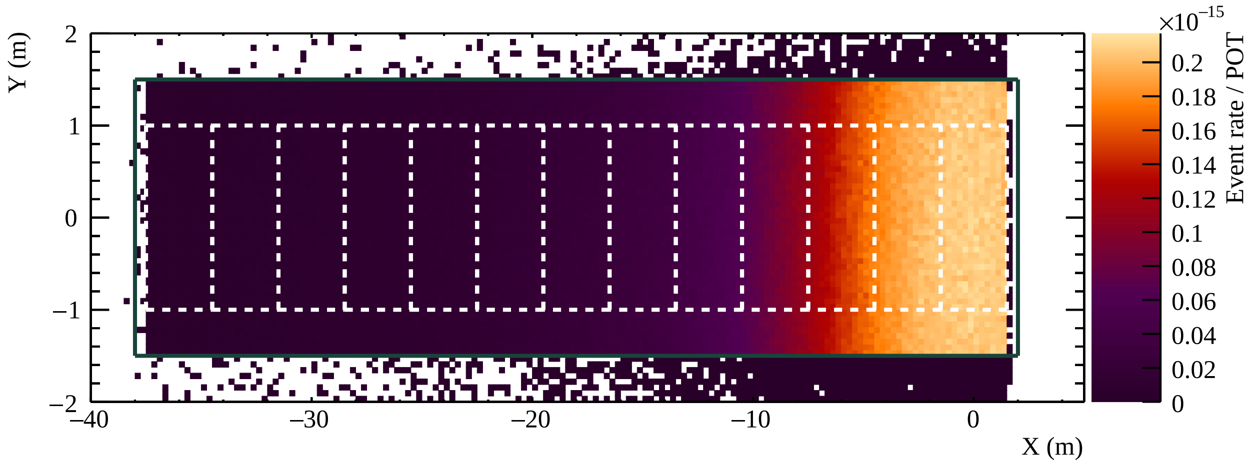

(a) X/Y projection of simulated interaction positions in the near detector

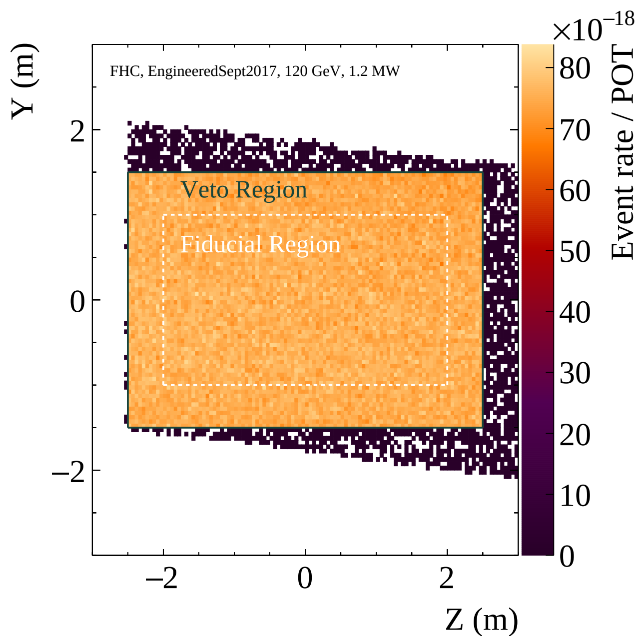

(b) Z/Y projection of simulated interaction positions in the near detector

Figure 24: The X/Y and Z/Y positions of simulated neutrino interaction positions within the near detector geometry. The fiducial and veto regions used in § 4 are overlaid. The interactions that occur outside of the veto region occur on an air target.

B Veto region energy cut value

Detailed studies into acceptable visible deposits in a detector veto region would require a full detector simulation. In the interest of simplicity, an arbitrary 10 MeV of deposited energy in the veto region (*c.f.* § 4.3 and Figure 24) cut was used to define hadronic containment. To check that the conclusions of the studies presented in § 4.3 were not strongly dependent on this cut, similar plots were made for a strict 0 MeV cut and a slightly looser 20 MeV restriction. It can be seen in Figure B that the efficiency is not strongly sensitive to the value of a non-zero energy deposit cut.

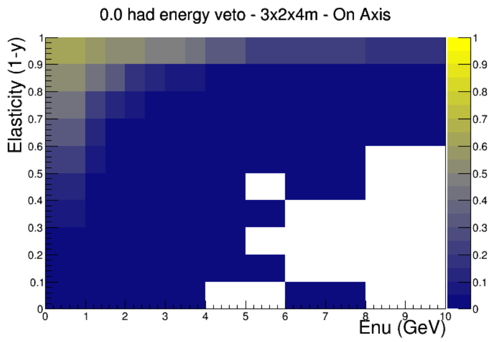

(a) 0 MeV, on axis

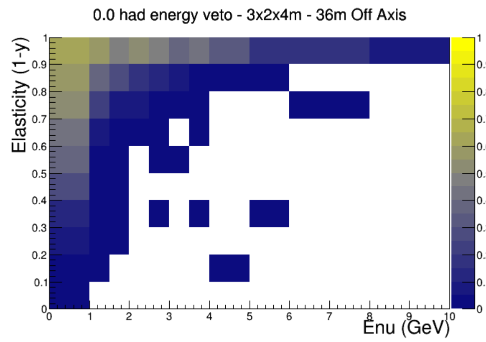

(b) 0 MeV, 36 m off axis

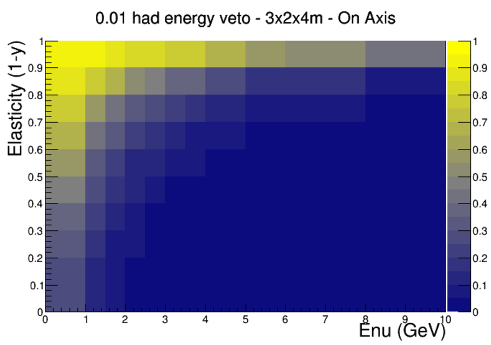

(c) 10 MeV, on axis

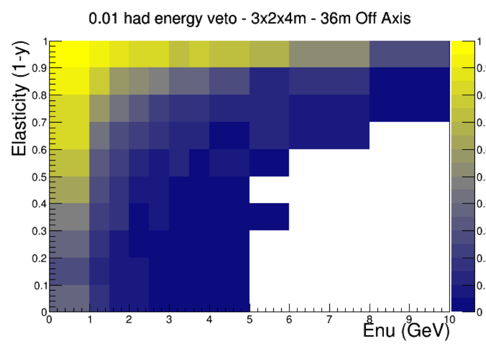

(d) [10 MeV, 36 m off axis

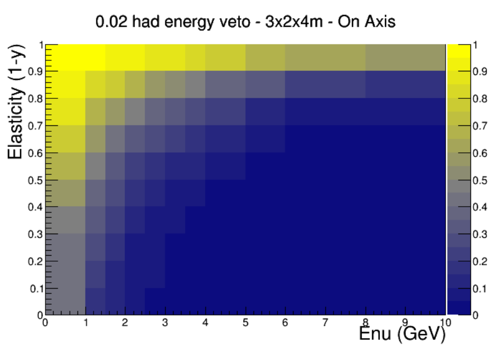

(e) 20 MeV, on axis

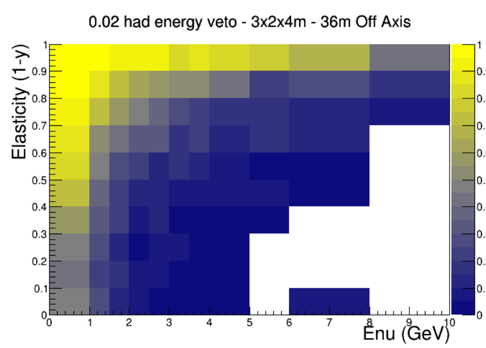

(f) 20 MeV, 36 m off axis

Figure 25: The selection efficiency for contained hadronic events in the samples described in § 4.3 at the on axis and 36 m off axis detector stops for three values of the veto region visible energy cut. It is clear that a strict cut of 0 MeV qualitatively changes the overall efficiency, the difference between a cut of 10 MeV and 20 MeV is small.

C Muon toplogy and hadronic containment

The effect of the combined muon containment (*c.f.* § 4.2) and hadronic containment (*c.f.* § 4.3) cuts on the selection efficiency as a function of neutrino energy and energy transfer is shown in Figure C. As might be expected, the requirement that the muon is contained prefers low energy, low elasticity events. Requiring that the muon exits with 50 MeV or more of kinetic energy prefers more elastic, higher energy events that results in energetic muons and comparatively small hadronic showers.

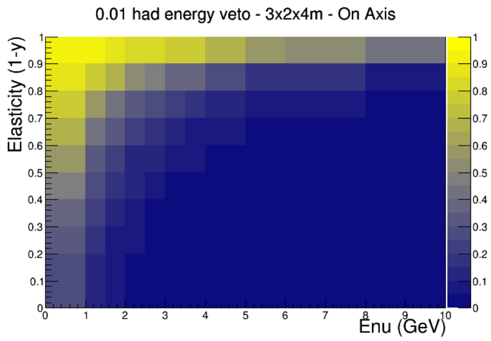

(a) on axis

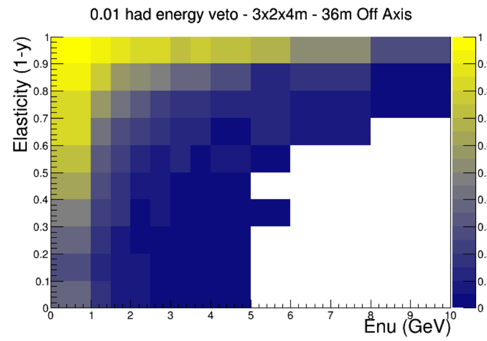

(b) 36 m off axis

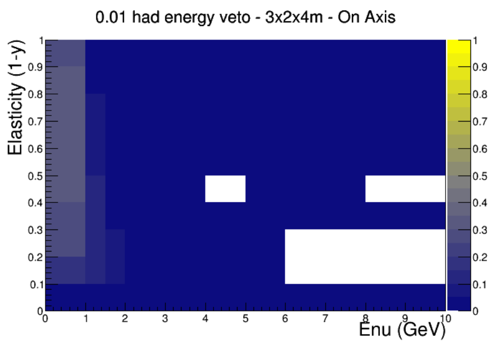

(c) μ containment, on axis

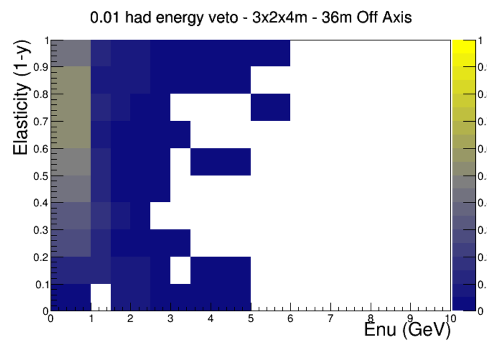

(d) μ containment, 36 m off axis

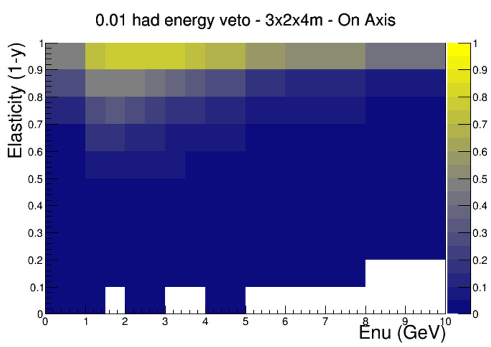

(e) μ exit, on axis

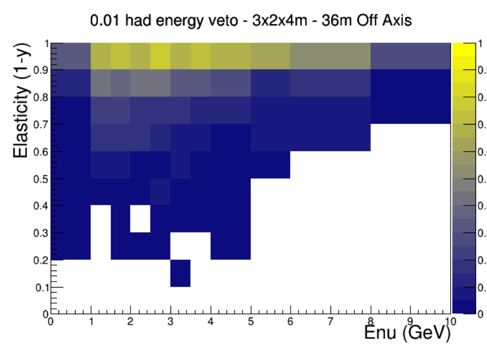

(f) μ exit, 36 m off axis

Figure 26: Comparison of the selection efficiency for contained hadronic events with no muon selection, the contained muon selection, and the exiting muon selection. Highly elastic events tend to result in a final state muon that exits the detector, while low energy events with lower elasticity tend to produce hadronic showers containable within the simulated fiducial region.

References

[1] L. Alvarez-Ruso *et al.*, "NuSTEC White Paper: Status and Challenges of Neutrino-Nucleus Scattering," arXiv:1706.03621 [hep-ph].

[2] U. Mosel, O. Lalakulich and K. Gallmeister, Phys. Rev. Lett. **112**, 151802 (2014) doi:10.1103/PhysRevLett.112.151802 [arXiv:1311.7288 [nucl-th]].

[3] A. M. Ankowski, P. Coloma, P. Huber, C. Mariani and E. Vagnoni, Phys. Rev. D **92**, no. 9, 091301 (2015) doi:10.1103/PhysRevD.92.091301 [arXiv:1507.08561 [hep-ph]].

[4] K. Abe *et al.* [T2K Collaboration], Phys. Rev. D **96**, no. 9, 092006 (2017) doi:10.1103/PhysRevD.96.092006 [arXiv:1707.01048 [hep-ex]].

[5] S. Bhadra *et al.* [nuPRISM Collaboration], arXiv:1412.3086 [physics.ins-det].

[6] `G4LBNF` project page: `https://cdcvs.fnal.gov/redmine/projects/lbne-beamsim/wiki`

[7] `PPFX` project page: `https://cdcvs.fnal.gov/redmine/projects/ppfx/wiki`

[8] `dk2nu` project page: `https://cdcvs.fnal.gov/redmine/projects/dk2nu/wiki`

[9] Near Detector Task Force Report and inputs `https://docs.dunescience.org/cgi-bin/private/ShowDocument?docid=1792`

[10] P. Madigan, LBNF beam alignment parameters and DUNE neutrino flux uncertainties, **DUNE-doc-1486-v1**: `https://docs.dunescience.org/cgi-bin/private/ShowDocument?docid=1486`.

[11] K. E. Duffy, "Measurement of the neutrino oscillation parameters sin223, m232, sin213, and CP in neutrino and antineutrino oscillation at T2K," doi:10.1007/978-3-319-65040-1

[12] L. Fields, Beam Alignment Tolerances and Systematic Uncertainties,**LBNE-doc-8410-v4**: `https://lbne2-docdb.fnal.gov/cgi-bin/private/ShowDocument?docid=8410`.

[13] Long-Baseline Neutrino Facility (LBNF) and Deep Underground Neutrino Experiment (DUNE) Conceptual Design Report Volume 3: Long-Baseline Neutrino Facility for DUNE June 24, 2015

arXiv:1601.05823 [physics.ins-det]